

**Synthesis of NaNiF_3 and its Composite with
Multi-Walled Carbon Nanotubes as Cathode
Materials for Aqueous Sodium-Ion Battery**



By

Muhammad Zain Bin Amjad

Reg. No. 00000275386

Session 2018-20

Supervised by

Dr. Naseem Iqbal

**US-Pakistan Center for Advanced Studies in Energy
(USPCAS-E)**

National University of Sciences and Technology (NUST),

H-12, Islamabad 44000, Pakistan

October 2021

Synthesis of NaNiF_3 and its Composite with Multi-Walled Carbon Nanotubes as Cathode Materials for Aqueous Sodium-Ion Battery



By

Muhammad Zain Bin Amjad

Reg. No. 00000275386

Session 2018-20

Supervised by

Dr. Naseem Iqbal

**A Thesis Submitted to the US-Pakistan Center for Advanced Studies
in Energy in partial fulfillment of the requirements for the degree of**

**MASTER of SCIENCE in
Energy Systems Engineering**

US-Pakistan Center for Advanced Studies in Energy (USPCAS-E)

National University of Sciences and Technology (NUST),

H-12, Islamabad 44000, Pakistan

October 2021

THESIS ACCEPTANCE CERTIFICATE

Certified that final copy of MS/MPhil thesis written by **Mr. Muhammad Zain Bin Amjad (Registration No. 00000275386)**, of USPCASE has been vetted by undersigned, found complete in all respects as per NUST Statues/Regulations, is within the similarity indices limit and is accepted as partial fulfillment for the award of MS/MPhil degree. It is further certified that necessary amendments as pointed out by GEC members of the scholar have also been incorporated in the said thesis.

Signature: _____

Name of Supervisor: Dr. Naseem Iqbal

Date: _____

Signature (HoD): Dr. Rabia Liaqat

Date: _____

Signature (Dean/Principal): Dr. Adeel Waqas

Date: _____

Certificate

This is to certify that work in this thesis has been carried out by **Mr. Muhammad Zan Bin Amjad (Reg. No. 00000275386)** and completed under my supervision in Synthesis and Energy Storage & Conservation Laboratory, US-Pakistan Center for Advanced Studies in Energy (USPCAS-E), National University of Sciences and Technology, H-12, Islamabad, Pakistan.

Supervisor:

Dr. Naseem Iqbal
USPCAS-E
NUST, Islamabad

Co-Supervisor

Dr. Ghulam Ali
USPCAS-E
NUST, Islamabad

GEC member 1:

Dr. Mustafa Anwar
USPCAS-E
NUST, Islamabad

GEC member 2:

Dr. Sehar Shakir
USPCAS-E
NUST, Islamabad

HOD-ESE:

Dr. Rabia Liaqat
USPCAS-E
NUST, Islamabad

Dean/Principal:

Dr. Adeel Waqas
USPCAS-E
NUST, Islamabad

Dedication

To my beloved Parents and Teachers who have supported in every aspect of my life.

ABSTRACT

Aqueous sodium-ion battery is a safe and efficient system for large-scale energy storage due to its low cost, abundant sodium supply, non-flammable aqueous neutral electrolyte, and quick charge-discharge performance. The usage of fluoride-based materials as electrode materials offers several advantages due to their high potential window and energy density. Exploring perovskite materials offers the benefit of a corner-sharing matrix structure, which aids in ion and electron transport. We used a simple and cost-effective method of precipitation and hydrothermal synthesis to create the perovskite-structured NaNiF_3 and its composite with multi-walled carbon nanotubes (MWCNT). The synthesized material is characterized by X-ray diffractometry (XRD), scanning electron microscopy (SEM), energy dispersive X-ray (EDX), thermogravimetric analysis (TGA), and Brunauer-Emmett-Teller analysis (BET). Using 1 M Na_2SO_4 as electrolyte, cyclic voltammetry (CV), chronopotentiometry (CP), and electrochemical impedance spectroscopy (EIS) are used to evaluate the electrochemical performance of cathode material for aqueous sodium-ion battery. XRD confirms the perovskite structure of NaNiF_3 and $\text{NaNiF}_3 // \text{MWCNT}$, SEM shows the orthorhombic cube and cubical structure of NaNiF_3 and $\text{NaNiF}_3 // \text{MWCNT}$. The electrochemical results show that NaNiF_3 and $\text{NaNiF}_3 // \text{MWCNT}$ have excellent performance with specific capacities of 33 mAh g^{-1} and 57 mAh g^{-1} at 0.1 A g^{-1} and shows 16 Wh kg^{-1} and 28 Wh kg^{-1} energy density respectively and excellent cyclic stability up to 500 cycles, indicating that $\text{NaNiF}_3 / \text{MWCNT}$ is a potential candidate as cathode material for aqueous sodium.

Keywords: Aqueous Sodium-Ion Battery, Sodium Metal Fluoride, Transition Metal Fluoride, Sodium-ion Battery, Cathode Material.

Table of Contents

ABSTRACT	V
LIST OF FIGURES	IX
LIST OF TABLES	XI
LIST OF PUBLICATIONS	XII
LIST OF ABBREVIATIONS/NOMENCLATURE	XIII
CHAPTER 1 INTRODUCTION	1
1.1 Introduction	1
1.2 Energy storage	2
1.2.1 Energy storage technologies	4
1.2.1.1 Thermal energy storage (TES) systems:	4
1.2.1.2 Mechanical energy storage.....	4
1.2.1.2.1 Flywheel system	4
1.2.1.2.2 Pumped hydro storage system (PHSS).....	5
1.2.1.3 Electrical energy storage systems (EESS)	5
1.2.1.3.1 Capacitor.....	6
1.2.1.3.2 Supercapacitor	6
1.2.1.3.3 Superconducting magnetic energy storage.....	6
1.2.1.4 Chemical energy storage systems	7
1.2.1.4.1 Hydrogen	7
1.2.1.4.2 Synthetic natural gas (SNG).....	7
1.2.1.4.3 Biofuels.....	7
1.2.1.5 Electrochemical energy storage	8
1.2.1.5.1 Primary battery	8
1.2.1.5.2 Secondary battery	8
1.2.1.5.3 Fuel cell	8
1.2.1.5.4 Reserve cell.....	9
1.2.1.5.5 Rechargeable Batteries	9
1.3 Sodium Ion batteries	9
1.3.1 Comparison between Sodium and Lithium.....	11

1.3.2 Aqueous sodium Ion batteries.....	11
Summary:.....	15
References:	16
CHAPTER 2 LITERATURE REVIEW	18
2.1 Aqueous Sodium Ion Battery	18
2.2 Transition Metal Fluorides	20
2.3 Sodium Nickel Fluoride.....	21
2.3.1 Synthesis methods.....	21
2.3.2 Electrochemical Performance	22
Summary:.....	24
References:	25
CHAPTER 3 EXPERIMENTATION AND CHARACTERIZATION	28
3.1 Synthesis Method	28
3.1.1 Precipitation Route.....	28
3.1.2 Hydrothermal Route.....	28
3.2 Material Characterization Techniques.....	29
3.2.1 X-Ray Diffraction	29
3.2.2 Scanning Electron Microscopy	30
3.2.3 Energy Dispersive X-Ray Spectroscopy.....	31
3.2.4 Thermogravimetric Analysis	32
3.2.5 BET	33
3.3 Electrochemical Characterization.....	34
3.3.1 Suspension formation & Electrolyte.....	34
3.3.2 Cyclic Voltammetry (CV).....	35
3.3.3 Chronopotentiometry (CP).....	37
3.3.4 Electrochemical Impedance Spectroscopy	38
Summary:.....	40
References.....	41
CHAPTER 4 METHODOLOGY AND EXPERIMENTATION	43
4.1 Materials	43
4.2 Synthesis of NaNiF_3	43

4.3 Synthesis of NaNiF_3 // MWCNT.....	44
4.4 Material Characterization	45
4.5 Electrochemical Characterization.....	45
Summary:.....	46
References:	47
CHAPTER 5 RESULTS & DISCUSSION	48
5.1 Material Characterization	48
5.1.1 X-Ray Diffraction	48
5.1.2 Scanning Electron Microscopy	49
5.1.3 Energy Dispersive X-Ray Spectroscopy.....	50
5.1.4 Thermogravimetric Analysis	52
5.1.5 BET	52
5.2 Electrochemical Characterization.....	55
5.2.1 Cyclic Voltammetry.....	55
5.2.2 Chronopotentiometry	57
5.2.3 Electrochemical Impedance Spectroscopy	59
5.2.4 Cyclic Stability.....	61
5.3 Discussion.....	63
Summary:.....	65
References:	66
CHAPTER 6 CONCLUSION AND RECOMENDATIONS	68
6.1 Conclusion.....	68
6.2 Recommendations	68
ACKNOWLEDGMENTS	70
APPENDIX 1-PUBLICATIONS	71

List of Figures

Figure 1.1 Proportion of Renewable Energy Currently used World Wide [4].	2
Figure 1.2 Comparison of energy storage systems power output and module size [10].	3
Figure 1.3 Schematic of pumped hydro energy storage system [4].	5
Figure 1.4 Charge storage mechanism of supercapacitor [12].	6
Figure 1.5 Schematic diagram of fuel cell energy storage system [4].	9
Figure 1.6 Energy storage mechanism of sodium ion battery [6].	10
Figure 1.7 Development History of rechargeable batteries [17].	12
Figure 1.9 Schematic Mechanism of Aqueous Sodium Ion battery.	12
Figure 1.10 Energy density of different rechargeable batteries [8].	14
Figure 3.1 Autoclave used for the hydrothermal synthesis technique.	29
Figure 3.2 Schematic of X-Rays diffraction Process.	30
Figure 3.3 Schematic drawing of the scanning electron microscopy.	31
Figure 3.4 Schematic mechanism of energy dispersive X-Ray spectroscopy.	32
Figure 3.5 Schematic of TGA.	33
Figure 3.6 Schematic mechanism of BET.	34
Figure 3.7 Electrochemical Workstation.	35
Figure 3.8 3 Electrode System Configuration (Retrieved from Electrochemical cell and electrodes for cyclic voltammetry, Demonstration by Dr. Alf Bacher; notes by Shadi Rezai)	35
Figure 3.9 Cyclic Voltammetry [17].	36
Figure 3.10 Chrono-potentiometry [17].	37
Figure 3.11 Electrochemical Impedance Spectroscopy [17].	39
Figure 4.1 Schematic for synthesis of NaNiF_3 .	44
Figure 4.2 Schematic for synthesis of NaNiF_3 composite with MWCNT.	45
Figure 5.1 XRD patterns of synthesized NaNiF_3 , MWCNT, and $\text{NaNiF}_3 // \text{MWCNT}$.	49
Figure 5.2 SEM images of (a) NaNiF_3 , (b) NaNiF_3 , (c) MWCNT and (d) $\text{NaNiF}_3 // \text{MWCNT}$.	50
Figure 5.3 EDS spectra of (a) NaNiF_3 , and (b) $\text{NaNiF}_3 // \text{MWCNT}$.	51
Figure 5.4 Thermogravimetric analysis curves of NaNiF_3 and $\text{NaNiF}_3 // \text{MWCNT}$.	52

Figure 5.5 N ₂ Adsorption-desorption isotherms (inset graph of BJH pore size distribution) of (a) NaNiF ₃ and (b) NaNiF ₃ // MWCNT.	54
Figure 5.6 Cyclic Voltammetry curves of (a) NaNiF ₃ , (b) NaNiF ₃ // MWCNT and (c) Comparison of CV of NaNiF ₃ and NaNiF ₃ // MWCNT.	56
Figure 5.7 . Represents the galvanic charge-discharge curves of (a) NaNiF ₃ (b) NaNiF ₃ // MWCNT, (c) GCD curve comparison between NaNiF ₃ and NaNiF ₃ // MWCNT.	58
Figure 5.8 Represents the electrochemical impedance spectroscopy (a) Nyquist plot of NaNiF ₃ and NaNiF ₃ // MWCNT with inset equivalent fitted circuit and (b) Bode plot of NaNiF ₃ and NaNiF ₃ // MWCNT.	60
Figure 5.9 (a) Specific capacitance at each scan rate for initial 5 cycles each of NaNiF ₃ and NaNiF ₃ // MWCNT (b) Cyclic stability at 1 A g ⁻¹ of NaNiF ₃ and NaNiF ₃ // MWCNT (c) Comparison of specific capacity and coulombic efficiency at each scan rate of NaNiF ₃ and NaNiF ₃ // MWCNT.	62

List of Tables

Table 2.1 Recent cathode materials used for aqueous sodium ion battery.	20
Table 5.1 Elemental composition of NaNiF_3 and $\text{NaNiF}_3 // \text{MWCNT}$	51
Table 5.2 BET Pore volume, surface area and average pore radius of NaNiF_3 and $\text{NaNiF}_3 // \text{MWCNT}$	53
Table 5.3 Comparison of this study with recent. literature.	64

List of Publications

- **M. Zain Bin Amjad**, Naseem Iqbal, Ghulam Ali, Tayyaba Noor, Ahmed A. Qayyum, Usman Ali Khan, Waqas Nazar, “**Synthesis of NaNiF_3 and its Composite with Multi-Walled Carbon Nanotubes as Cathode Materials for Aqueous Sodium-Ion Battery**” (Under-Review in Journal of Electroanalytical Chemistry)
- Mahrukh Khan, Humera Farah, Dr. Naseem Iqbal, Tayyaba Noor, **M Zain Bin Amjad**, Syeda Sidrah Ejaz Bukhari, “ **TiO_2 composite with graphitic carbon nitride as photocatalyst for biodiesel production from waste cooking oil**” (Accepted in RSC Advances)
- Rimsha Mehek, Naseem Iqbal, Tayyaba Noor, **M. Zain Bin Amjad**, Ghulam Ali, and M. Abdullah Khan, “**Metal–organic framework-based electrode materials for lithium-ion batteries: a review**”. *RSC Adv.*, 2021,11, 29247-29266
- Usman Ali Khan, Naseem Iqbal, Tayyaba Noor, Rabia Ahmad, Awais Ahmad, Junkuo Gao, **Zain Amjad** and Abdul Wahab, “**Cerium based metal organic framework derived composite with reduced graphene oxide as efficient supercapacitor electrode**”. *Journal of Energy Storage*, 41, 2021, 102999.

List of Abbreviations/Nomenclature

MWCNT	Multi-Walled Carbon Nano-Tubes
XRD	X-Rays Diffraction
SEM	Scanning Electron Microscopy
TGA	Thermogravimetric Analysis
BET	Braunner Emmett Teller
EDS	Energy Dispersive X-ray Spectroscopy
LIB	Lithium-Ion Battery
SIB	Sodium Ion Battery
ASIB	Aqueous Sodium Ion Battery
CP	Chronopotentiometry
GCD	Gravimetric Charge Discharge
CV	Cyclic Voltammetry
EIS	Electrochemical Impedance Spectroscopy
TMF	Transition Metal Fluoride
SMF	Sodium Metal Fluoride
MOF	Metal Organic Frame Works
ZIF	Zeolitic Imidazolate Framework
ESS	Energy Storage System
SHE	Standard Hydrogen Electrode

CHAPTER 1 INTRODUCTION

1.1 Introduction

Despite the fact that the world's energy supply continues to grow, the fossil fuel share is steadily declining, indicating a growing concern about emissions reductions. Renewable energy will replace traditional fossil energy on a big scale in the future due to environmental goals, the growth trend of carbon dioxide emission reduction, the rise in oil costs, and the use of fossil energy.

Throughout history, energy has been one of the world's most challenging concerns and a crucial component in global growth. Unavoidable consequences include global warming. Human activities have contributed to a 1°C increase in global temperature during the past 120 years. Renewable energy will replace traditional fossil fuels in the future due to environmental aims and the trend of reducing carbon dioxide emissions, as well as rising oil costs and fossil fuel usage [1]. As a result of renewable energy's unpredictability and inconsistency, there will be operational hazards to power systems, such as frequency and voltage stability problems. An energy storage technology system (ESS) is often considered as a viable solution to this problem due to its growing popularity and integration with intermittent renewable energy sources. Due to the energy storage, renewable energy sources and the grid can operate together more effectively. There are three operating states for the ESS in the power system: charging, storing, and discharging, and they are all separately managed. It can store energy created in the power system and transmit it back when needed. The value of fossil fuels has been steadily declining over the past few years as a result of intensive industrial development. People will be concerned about energy storage technologies in the future. Electricity, among other forms of energy, satisfies the human need for sustainable development. A key problem, however, is the lack of reliable power storage. Expanding storage capacity is still a long way off. In recent years, the need for high-performance rechargeable batteries has grown [2], [3]. Fig. 1.1 represents the proportion of renewable energy mainly used in the world [4].

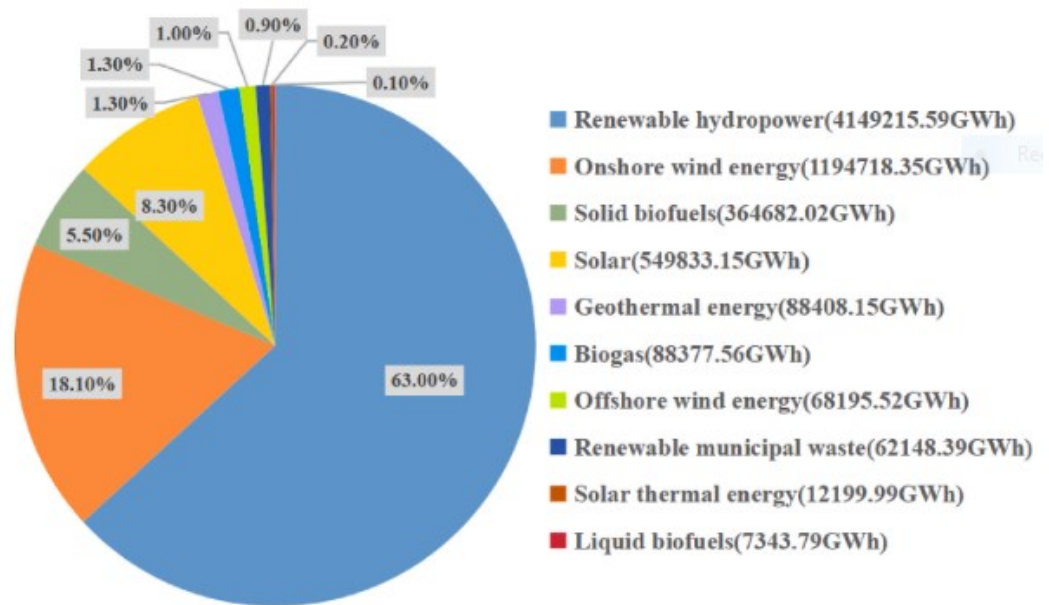


Figure 1.1 Proportion of Renewable Energy Currently used World Wide [4].

Batteries with long-term stability, high cycle life, and environmental friendliness are important criteria for contemporary electrochemistry in order to flourish. Batteries must have a low discharge rate, a high energy density, a high operating voltage, no memory effect, and environmental safety. Lithium-ion battery technology is well established, but there are still worries regarding their safety and cost. Lithium battery costs will continue to grow due to the increasing demand for Li commodity chemicals and the limited availability of Li ore sources. Lithium supplies may be depleted in the near future due to the extensive usage of Li ion batteries for traction purposes in particular scenarios[5]. Low-cost and widely available sodium-based batteries have the potential to satisfy the demands of large-scale grid energy storage. Some businesses may find it advantageous to use batteries based on sodium since it is so abundant (4th most abundant element on Earth's surface). Only in the United States are there 23 billion tonnes of soda ash. Large-scale battery applications can benefit from the abundance and low cost (about \$135–165/tonne) of trona, which is a sodium salt that is less expensive than lithium carbonate (around \$5000/tonne in 2010) [6], [7], [8].

1.2 Energy storage

In most situations, electrical energy is a cheap and easily available commodity that is invisible to the naked eye. Historically, it has been regarded as a common

consumer as fossil fuels are depleted, renewable sources of energy are being used, and environmental concerns are developing, it currently accounts for 12 % of the total energy handled by mankind. This percentage is anticipated to rise over the next several years, reaching 34 percent by 2025. Electricity is currently produced in a very centralized manner, sometimes at a distance from its final consumers. Initially, load balancing relies upon daily and seasonal forecasts, but it also relies on auxiliary modes such as hydraulic and thermal plants when production is insufficient. A very low-cost primary energy source will be transformed into an intermediate energy source, this will be stored and utilized at a later date to substitute expensive main power used in peak-load power plants or "virtual energy" that can be imposed as a result of a failure. As a result, the current transmission and distribution infrastructure may be used for many years to come. Due to kinetic advantages of future energy storage and retrieval systems, they will be able to give immediate reaction to demand. As a result, they will be able to supply greater network temporary production deficits, which may be foreseen, can produce a network imbalance. Alternatively, production problems might be the cause of the requirement. In order to make up for the expenses of a double-conversion chain, the profits attributable to storage systems must be substantial [9], [10], [4]. Fig. 1.2 Represent a comparison of ESS's power output and module size.

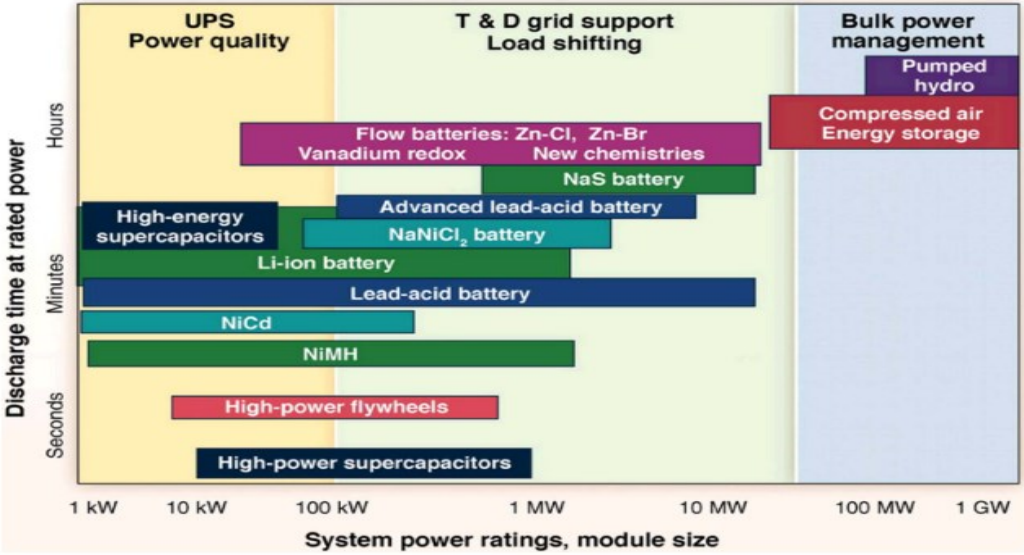


Figure 1.2 Comparison of energy storage systems power output and module size [10].

1.2.1 Energy storage technologies

It is possible to store electricity efficiently, in the beginning, it must be converted into another type of energy that can be stored and re-converted as needed. Mechanical, chemical, and thermal energies may all be stored in a variety of ways. A wide range of storage methods are available, depending on the precise technological and economic conditions that must be met. Thermal energy, mechanical, electrical, chemical, and electrochemical energy storage systems are some of the most common types of ESS [10], [4], [11].

1.2.1.1 Thermal energy storage (TES) systems:

Thermal energy storage (TES) is a technique for storing heat or cold at a specified temperature in a storage medium for later use in a number of scenarios. In both the industrial and household sectors including hot water production, Space heating and cooling, regulating the process temperature, hot water production, and power generation are all possible with TES systems. TES systems include latent heat, sensory heat, adsorption, and absorption systems [10], [4].

1.2.1.2 Mechanical energy storage

Mechanical energy storage is classified into four groups based on their operating principles: potential energy, Kinetic energy, forced springs and pressurized gas. Mechanical energy storage has the advantage of being able to immediately deliver energy for mechanical processes whenever it is needed. There are several techniques to transmit and store energy from water currents, tidal sources and waves using mechanical energy storage systems. Flywheel and pumped storage systems, as well as pressurized gas storage, are among their most used storage methods [10], [4], [11].

1.2.1.2.1 Flywheel system

Most current high-speed flywheel energy storage devices employ a massive spinning cylinder (a rim attached to a shaft) supported on a stator by magnetically levitated bearings. Mechanical energy, in the form of high-speed rotating kinetic energy of the rot, may be stored in a flywheel. When the flywheel slows down, kinetic energy may be returned to the electrical motor, which acts as a generator. [10].

1.2.1.2.2 Pumped hydro storage system (PHSS)

In pumped storage systems water is shifted between two reservoirs at different heights levels while storing and generating electricity. Pumped hydro energy storage devices enable the creation of large-scale energy reservoirs utilizing water. As a result, renewable energy sources like wind, solar, and wave power are increasingly relying on pumped storage to keep their outputs stable when they fluctuate. Because of the pumping mechanism, surplus generation (or negative load) can be held during periods of high production and low consumption, and then released [10], [11]. Fig. 1.3 represent the schematic diagram of Pumped hydro storage [4].

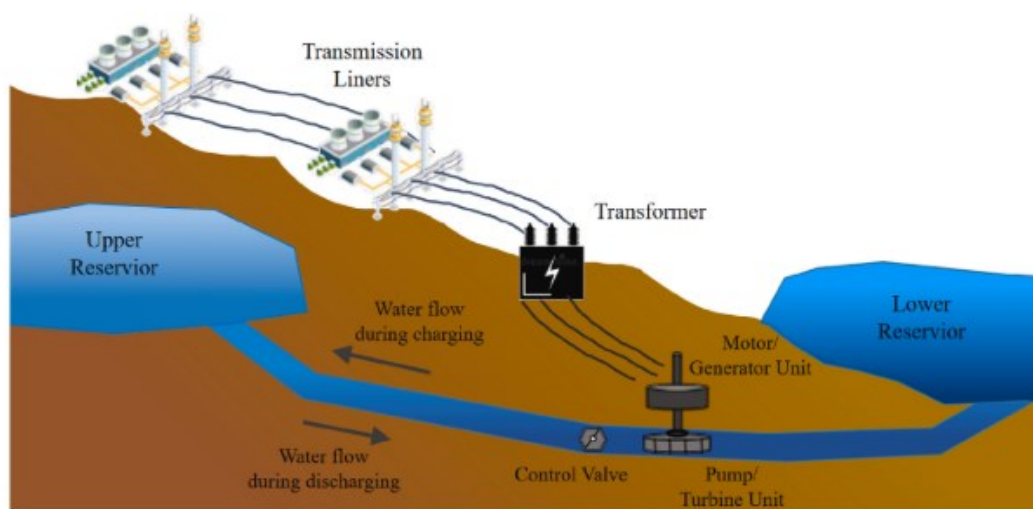


Figure 1.3 Schematic of pumped hydro energy storage system [4].

1.2.1.3 Electrical energy storage systems (EESS)

The two categories of electric energy storage systems are electrostatic (including capacitors and super capacitors) and magnetic/current storage systems (EESS). Super capacitors have a huge capacitance in a tiny package, they may be employed in place of regular capacitors, and superconducting magnetic energy storage devices can be utilized to stabilize output at the end of a power plant or in industrial settings. Super capacitors can replace regular capacitors except that they offer very high capacitance in a small package, and superconducting magnetic fields can be used in the case of high currents, but only for very short periods due to their relatively low capacitance generation [10], [4].

1.2.1.3.1 Capacitor

The most basic and easiest technique of storing electricity is via capacitors. In a capacitor, a dielectric layer separates two metal plates. A direct-current source charges one plate, while the other plate is charged in the opposite way. As a result, they store energy in the form of a metalized plastic film. Because capacitors have a relatively low energy density, they can supply or receive large currents, but only for very brief periods of time because of their low [10].

1.2.1.3.2 Supercapacitor

As an electrochemical double-layer capacitor known as a supercapacitor, they bridge the gap between traditional capacitors used in electronics. Electrolytes in supercapacitors are molecule-thin, and activated carbon structures have a high surface area. Supercapacitors have superior energy storage capacities as compared to ordinary capacitors. Static charge distinguishes supercapacitors from electrochemical batteries. They can also be re-charged and discharged, in addition to delivering a high peak power output (in contrast to batteries) [10]. Fig. 1.4 schematic diagram of charge storing mechanism of supercapacitor [12].

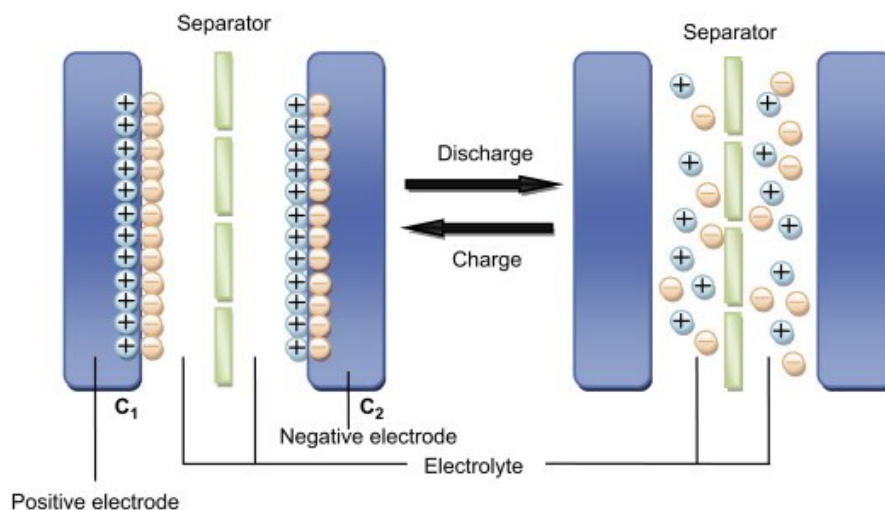


Figure 1.4 Charge storage mechanism of supercapacitor [12].

1.2.1.3.3 Superconducting magnetic energy storage

Electrodynamics underpins superconducting magnetic energy storage (SMES). The energy is stored in a magnetic field formed by direct current flowing through a superconducting coil that is maintained below the threshold temperature for

superconductivity. The stored energy may be released back into a network of superconducting material that has been cryogenically frozen [10].

1.2.1.4 Chemical energy storage systems

Chemical energy is created by chemical bonding in between molecules and atoms during a chemical process. After the energy (chemical) has been released, the material is typically transformed into a completely new one. In both electrical generating and energy transfer, chemical fuels are the most common way of storing energy, gasoline and propane are the most prevalent types of chemical fuels that are processed. Other fuels include hydrogen and biodiesel [10], [4].

1.2.1.4.1 Hydrogen

Hydrogen is a non-toxic, plentiful, and clean renewable fuel and energy carrier material. Water can be converted into hydrogen by thermolysis or electrolysis, fossil fuels can be reformed, biomass can be gasified and even methanol can be converted into hydrogen as well. As a result of the combustion event of hydrogen, it merely emits water with huge amount of energy as compared to other fossil fuels [10].

1.2.1.4.2 Synthetic natural gas (SNG)

The most often utilized gas fuel is natural gas, and it is made up mostly of CH₄. Other gas fuels include Bio-SNG, landfill gas, biogas and SNG. Organic matter decays to create biogas, which is composed of CH₄ and CO₂. Solid feedstock can be partially transformed to synthetic natural gas (SNG) via gasification, which is followed by conditioning [10].

1.2.1.4.3 Biofuels

Plant and animal-derived organic stuff is called biomass. Energy crops produced specifically for energy production, Agricultural waste and leftovers (including vegetal or animal substances), forestry, as well as associated sectors such as fisheries or aquaculture are all examples of biomass. It is possible to get biofuels in gaseous. Biofuels, such as alcohol fuels, biodiesel, biomass or pure vegetable oil can be used to replace hydrocarbon fuels. Through a variety of chemical processes plant or animal biomass, natural gas, coal and organic waste may all be transformed into short hydrocarbons that can be utilized in place of conventional hydrocarbon fuels [10].

1.2.1.5 Electrochemical energy storage

Chemical energy is converted into electrical energy via electrochemical power sources, a chemical reaction takes place between at least two reaction partners throughout this procedure. An electric current with a specified voltage and time can be used to extract the reaction's energy. Batteries and capacitors are two important branches of the electrochemical storage technology. Current electrochemical storage systems come in a wide variety of shapes and sizes depending on the kind of chemical reaction, structural characteristics. There are four types of electrochemical cells and batteries: The primary battery, the secondary battery, the reserve battery, and the fuel cell are the four types of cells. Deep-cycle batteries, which have fewer metal electrodes in their design, are also suitable and may be divided into two categories based on discharge depth: shallow and deep. The third classification is based on whether the electrolyte in the battery is flooded, moist, or sealed [10] [4].

1.2.1.5.1 Primary battery

Primary batteries are typically non-rechargeable. Almost all primary cells include electrolytes in the forms of separator or absorbent material, although Electrolyte types such as non-aqueous and aqueous might be used to classify main batteries [10].

1.2.1.5.2 Secondary battery

Secondary-stage cells or batteries are rechargeable by sending a current across their circuit in a opposite direction. The kind of electrolyte in rechargeable battery systems may be divided into two categories: aqueous and nonaqueous electrolytes, Aqueous lithium/sodium batteries, Examples of batteries include Alkaline zinc manganese Dioxide, nickel metal hydride, lead acid, and nickel-cadmium batteries are few examples of having aqueous electrolytes, few examples of nonaqueous electrolyte batteries include lithium ion, Sodium ion, metal air batteries [10].

1.2.1.5.3 Fuel cell

A fuel cell is a device that generates electricity primarily by releasing hydrogen or another fuel's chemical energy and converting it to electricity, they create power and heat, as fuel cells function by passing hydrogen and oxygen via the anode and cathode, respectively. Electrons and protons are formed from the hydrogen molecules at the anode site. An electrolyte membrane allows the protons to flow through, while

a circuit forces the electrons to pass through, creating an electric current and surplus heat. At Cathode water molecules are created when protons, electrons, and oxygen are combined with each other [10]. Fig. 1.5 schematic of fuel cell energy storage system [4].

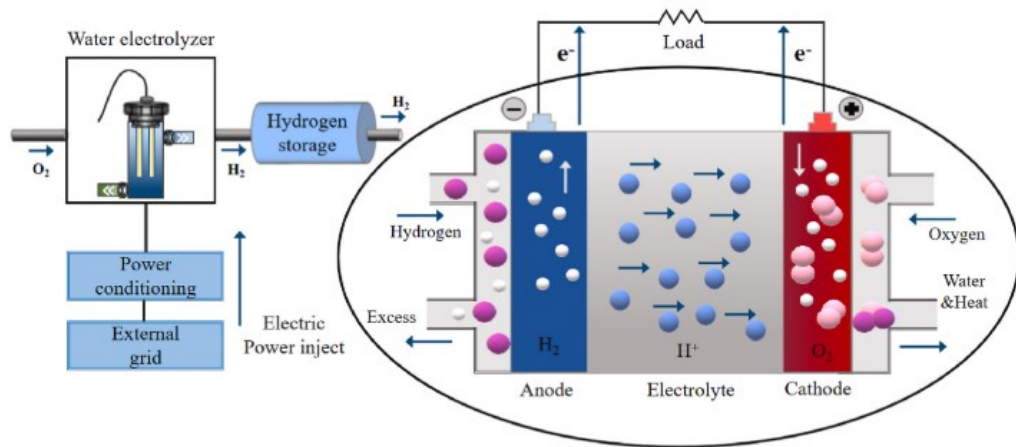


Figure 1.5 Schematic diagram of fuel cell energy storage system [4].

1.2.1.5.4 Reserve cell

As a type of primary battery, a reserve cell or battery falls. It is common to utilize reserve batteries in order to store energy, when not in use, the cell's active compounds are separated and kept. Assembling reserve batteries without electrolyte [10].

1.2.1.5.5 Rechargeable Batteries

There is no doubt that the most frequently utilized ESS technology is rechargeable batteries, such as lithium-ion batteries and Sodium Ion Batteries. When it comes to rechargeable batteries, the anode delivers electrons, while the cathode absorbs those. It is the separator's job to maintain the electrical isolation between the cathode and the anode, while the electrolyte is responsible for transferring electrons between the two electrodes [10].

1.3 Sodium Ion batteries

There is a rising need for electrochemical energy storage technology due to an increasing number of renewable energy sources and grid-scale battery applications. Due to resource constraints, lithium-ion batteries (LIBs) may not be able to fulfil this

large demand, despite the fact that their properties are ideal for almost every energy storage device requirement. You may compare them to lithium-ion batteries in terms of their characteristics (LIBs). Due to their natural composition, it is feasible to build battery modules that are less costly and more functional. There has been considerable progress in material production due to the high learning curve of the Lib-based technologies. Due to their low cost and abundance, sodium ion batteries (SIBs) are one of the most attractive alternatives due to their electrochemical and molecular similarities with lithium. Four decades after they were initially created using a similar working principle to LIBs, researchers began studying SIBs in earnest in 2010. They benefitted from the important information gained from LIBs research as well as from advances in nanotechnology [13], [12], [15]. The positive electrode or cathode active material delivers electrons to the external circuit during charging, oxidizing the transition metal ion. Part of the intercalated sodium atoms dissolve as ions in the electrolyte to maintain charge neutrality. They go to the negative electrode (anode), where they are intercalated into the structure to restore the charge neutrality that has been broken there by electrons provided and received from the cathode side. During discharge, the process is carried out in reverse. [16]. Fig. 1.6 represents the schematic of sodium ion battery [6].

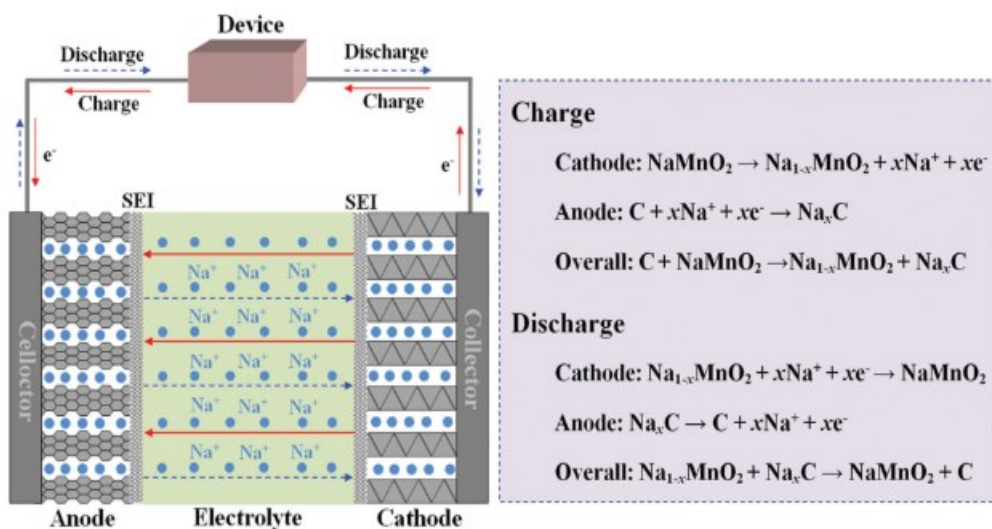


Figure 1.6 Energy storage mechanism of sodium ion battery [6].

1.3.1 Comparison between Sodium and Lithium

A major factor in the development of SIB technology is the success of LIBs, as well as the comparable chemical characteristics of Na and Li. Because of this, the SIB's quick expansion has been aided by years of knowledge and development of LIB technology. When it comes to energy storage technologies, sodium and lithium have long been considered equals. However, recent worries about the cost and availability of lithium in order to satisfy the ever-increasing EES needs have pushed researchers to resurrect this technique. Lithium and sodium are both elements in group 1 of the periodic table and belong to the same family. They're called alkali metals, and their valence shells have one loosely held electron. Consequently, alkali metals are very reactive, and as the group progresses their melting point decreases as well as their hardness, conductivity, and initial ionization energies. To compare two alkali elements, it's essential to look at their redox potential. In comparison to the standard reduction potential of Li^+/Li , Na^+/Na has a standard reduction potential of 2.71 V against SHE, which is roughly 330 mV higher. It is because of this that the anodic electrode potential for SIBs is always higher than that of a LIB. Both metals have a melting point, which is an essential physical feature to compare. A soft metal, Na has a melting temperature of just 96.7°C, whereas Li has a melting point of 180.5°C. Low melting point is a disadvantage when creating SIBs with a solid electrolyte conductivity considering how hot it must be for the conductivity to be functional [13], [7].

1.3.2 Aqueous sodium Ion batteries

There are no rechargeable battery options that can fulfil the application requirements of ESSs since they are not designed to do so. Recent interest in organic rechargeable devices has been sparked by their high energy density. Organic electrolyte has a few disadvantages. There are hazardous heavy metal components in lead-acid, Nickel–Cadmium, and Nickel–Metal Hydride traditional aqueous rechargeable systems. Vanadium and other aqueous batteries also constrained by high costs. Organic electrolyte is replaced by water electrolyte in aqueous sodium ion batteries. Figure 1.7 depicts the development of rechargeable batteries from their inception [17]. Fig. 1.8 shows the schematic mechanism of aqueous sodium ion battery.

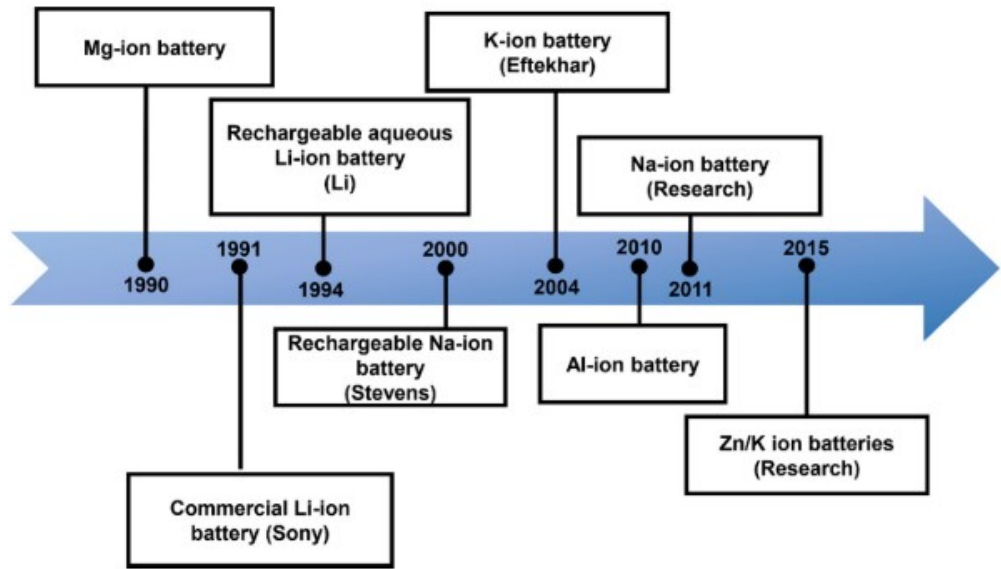


Figure 1.7 Development History of rechargeable batteries [17].

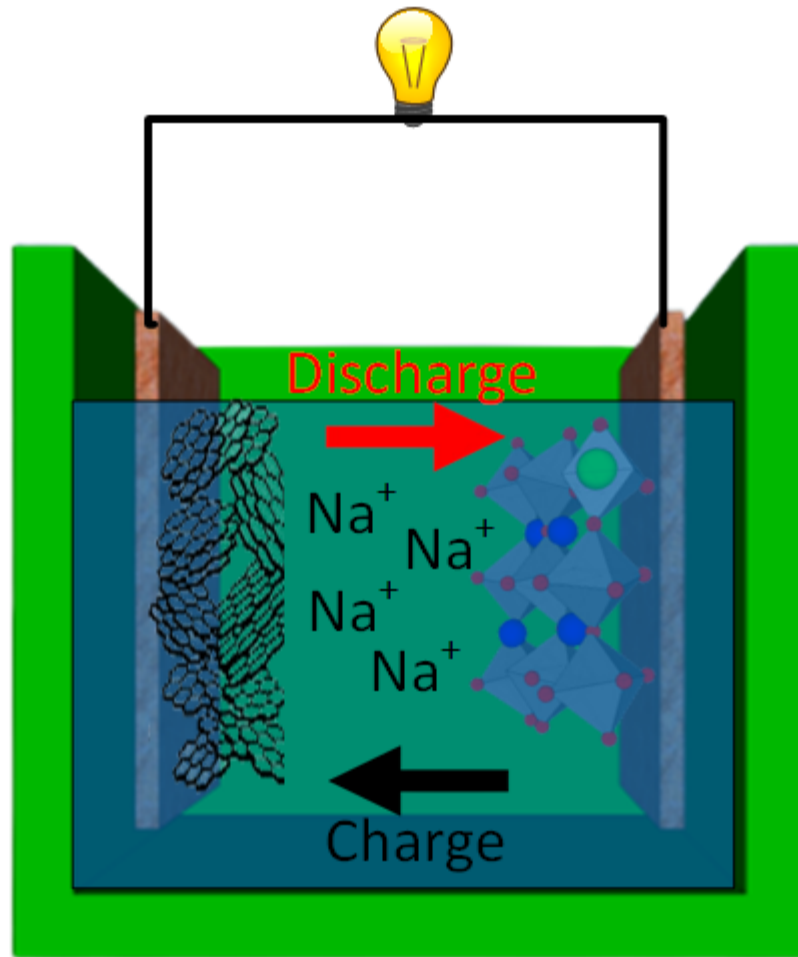


Figure 1.8 Schematic Mechanism of Aqueous Sodium Ion battery.

The development of a rechargeable aqueous battery still faces several challenges. It is important to note that, while it is possible to alter the voltage of dilute aqueous electrolyte by adjusting electrodes or adding additives, it is still significantly lower than that of organic electrolytes (mostly above 3 V). First of all, the interaction between aqueous electrolyte and the metal ions in it is complicated. When cycling, H^+ and metal ion exchange take place simultaneously, resulting in low specific capacity for the aqueous system. Element dissolution in aqueous electrolyte also affects capacity and stability. Additionally, the output and stability of aqueous battery systems are impacted by the electrolyte content, pH, oxygen concentration, and additives in the battery electrolyte. Because of the water decomposition process, aqueous electrolytes have a restricted electrochemical stability window (1.50 V) that limits the choice of electrochemical partners (cathode and anode materials) as well as the realistic energy output of such battery chemistries. Because of this, (i) there is a lack of good electrode materials that can be used in organic battery systems; (ii) Due to low voltage energy density is limited and (iii) sluggish side reaction between water and anode/cathode material will have a significant impact on cyclic stability. Fortunately, there is a way to overcome these challenges by combining dynamics and aqueous electrolyte, but there are still challenges. The cathode materials for aqueous sodium ion batteries have evolved over the past few years, including transition metal oxides (MnO_2 , Na_xMnO_2), analogues of Prussian blue, polyanionic compounds (NASICON materials, pyro-phosphate, phosphate, olivine type materials fluorinated pyrophosphate, etc.) and other Na-based compounds. [8], [17], [15]. Fig. 1.8 describe different battery technologies in terms of energy density [8].

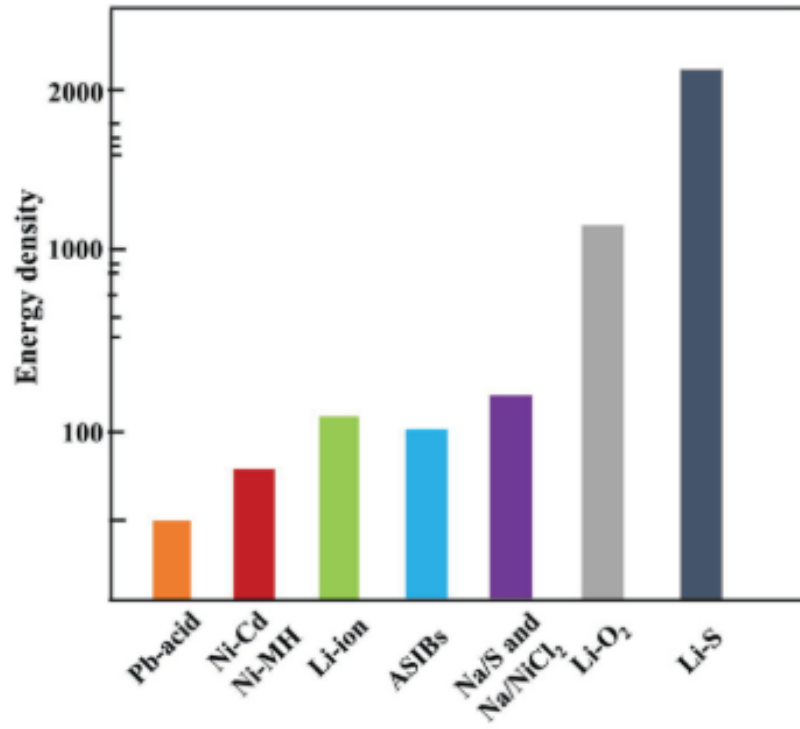


Figure 1.9 Energy density of different rechargeable batteries [8].

Summary:

Initially, the chapter discusses the global energy trend toward renewable sources of energy and energy storage systems, supported by energy storage technologies, with a focus on electrochemical energy storage on rechargeable and sodium ion batteries, as well as their comparison with lithium-ion batteries, which are discussed. Aqueous sodium ion batteries are also discussed in this chapter.

References:

- [1] M. M. Rafique and S. Rehman, "National energy scenario of Pakistan – Current status, future alternatives, and institutional infrastructure: An overview," *Renew. Sustain. Energy Rev.*, vol. 69, no. October 2016, pp. 156–167, 2017.
- [2] L. S. Martins, L. F. Guimarães, A. B. Botelho Junior, J. A. S. Tenório, and D. C. R. Espinosa, "Electric car battery: An overview on global demand, recycling and future approaches towards sustainability," *J. Environ. Manage.*, vol. 295, no. March, 2021.
- [3] T. Jin *et al.*, "High-Energy Aqueous Sodium-Ion Batteries," *Angew. Chemie - Int. Ed.*, vol. 60, no. 21, pp. 11943–11948, 2021.
- [4] Z. Zhang *et al.*, "A review of technologies and applications on versatile energy storage systems," *Renew. Sustain. Energy Rev.*, vol. 148, no. May, 2021.
- [5] B. Scrosati, "History of lithium batteries," *J. Solid State Electrochem.*, vol. 15, no. 7–8, pp. 1623–1630, 2011.
- [6] X. Xiang, K. Zhang, and J. Chen, "Recent advances and prospects of cathode materials for sodium-ion batteries," *Adv. Mater.*, vol. 27, no. 36, pp. 5343–5364, 2015.
- [7] J. Y. Hwang, S. T. Myung, and Y. K. Sun, "Sodium-ion batteries: Present and future," *Chem. Soc. Rev.*, vol. 46, no. 12, pp. 3529–3614, 2017.
- [8] D. Bin *et al.*, "Progress in Aqueous Rechargeable Sodium-Ion Batteries," *Adv. Energy Mater.*, vol. 8, no. 17, pp. 1–31, 2018.
- [9] F. R. McLarnon and E. J. Cairns, "Energy storage," 1989.
- [10] M. S. Guney and Y. Tepe, "Classification and assessment of energy storage systems," *Renew. Sustain. Energy Rev.*, vol. 75, no. November 2016, pp. 1187–1197, 2017.
- [11] H. Ibrahim, A. Ilinca, and J. Perron, "Energy storage systems-Characteristics and comparisons," *Renew. Sustain. Energy Rev.*, vol. 12, no. 5, pp. 1221–1250, 2008.

- [12] “Supercapacitor - Energy Education.” [Online]. Available: <https://energyeducation.ca/encyclopedia/Supercapacitor>. [Accessed: 10-Sep-2021].
- [13] K. Chayambuka, G. Mulder, D. L. Danilov, and P. H. L. Notten, “Sodium-Ion Battery Materials and Electrochemical Properties Reviewed,” *Adv. Energy Mater.*, vol. 8, no. 16, pp. 1–49, 2018.
- [14] W. Zhang, F. Zhang, F. Ming, and H. N. Alshareef, “Sodium-ion battery anodes: Status and future trends,” *EnergyChem*, vol. 1, no. 2, p. 100012, 2019.
- [15] D. Choi, S. Lim, and D. Han, “Advanced metal–organic frameworks for aqueous sodium-ion rechargeable batteries,” *J. Energy Chem.*, vol. 53, pp. 396–406, 2021.
- [16] T. Perveen, M. Siddiq, N. Shahzad, R. Ihsan, A. Ahmad, and M. I. Shahzad, “Prospects in anode materials for sodium ion batteries - A review,” *Renew. Sustain. Energy Rev.*, vol. 119, no. June 2019, p. 109549, 2020.
- [17] D. Yang *et al.*, “Pathways towards high energy aqueous rechargeable batteries,” *Coord. Chem. Rev.*, vol. 424, 2020.

CHAPTER 2

LITERATURE REVIEW

2.1 Aqueous Sodium Ion Battery

Practical application for energy storage system should be safe, have high cycle life, less cost, availability of raw material, environmentally friendly. Organic electrolytes are utilised in commercially available batteries for energy storage devices, which gives them a high energy density. Organic electrolytes used are hazardous, flammable and has a poor ion migration rate. These necessitates the replacement of extremely poisonous and combustible organic solvents with aqueous electrolytes (salts in water electrolytes), results in quick development aqueous ion batteries. Nickel metal hydride, Lead-acid and nickel Cadmium are some conventional aqueous rechargeable systems commercially available and but they contain harmful heavy metal elements which makes them unfit for environment. The environmental friendliness, low cost, ease of production, high safety, and ease of recycling, aqueous rechargeable batteries are potential alternatives for energy storage systems for large scale application. The aqueous neutral electrolyte also avoids the tough and high production cost and circumstances [1].

Water is an appealing non-aqueous solvent option since it is not only fundamentally safe, it's also a great solvent with a lot of acceptors and donors [2]. The low voltage platform limits the energy density of aqueous batteries, and will greatly influence the cyclic stability of an aqueous electrolyte's voltage window, even when the kinetics are taken into account. The limited stable voltage window means that a large number of excellent electrode materials for organic battery systems cannot be used. From previous study, it is clear that the fundamental component of aqueous batteries is their electrolytes, which may be viewed as a performance enhancer for electrochemical systems. Since water has a high dielectric constant, strong ionic conductivity, low vapour pressure, low viscosity and is intrinsically safe, it is an appealing alternative to organic solvents (such as ethylene carbonate, or EC). It is possible to utilise either diluted electrolyte or concentrated electrolyte, depending on

the anode/cathode composition [2]. Electrolytes that are concentrated or gel electrolytes may be used to increase the electrochemical stability window. The majority of high-voltage full-cell systems have low cycle stability and coulomb efficiency, according to research. Extending the voltage window for a complete cell and selecting high-capacity electrode materials are necessary for the development of high-voltage aqueous sodium ion batteries [3]. In an aqueous electrolyte, the process of electrochemical sodium insertion and de-insertion is more difficult, which makes the electrode material selection procedure more difficult. Aqueous electrolytes require electrode materials with redox potentials close to or equal to those of water, beyond which water electrolysis results in O₂ or H₂ evolution. First and foremost: cyclic stability is affected by the side reactions of anode/cathode with water or residual O₂ [3].

Rechargeable batteries with an aqueous electrolyte are categorised as Na⁺, Li⁺, Zn²⁺, K⁺, Mg²⁺, Ca²⁺, Al³⁺, or Cl-ion aqueous batteries depending on the type of principal charge carrier [4]. Lithium-based rechargeable batteries, including lithium ion, lithium air, and lithium sulphur, have been extensively researched to meet the need for energy storage devices. Some battery choices, such as sodium ion, potassium ion, magnesium and aluminium ion, have become feasible alternatives owing to worries about cost and the depletion of lithium supplies due to increased demand [5]. Rechargeable batteries using aqueous metal-ion electrodes, Organic and Prussian blue analogues has been studied, as well as traditional electrode materials such as oxide and polyanionic compounds and their derivatives [4], [2]. Due to the safety, low cost, environmental friendliness, and long lifespan, aqueous sodium ion batteries have a lot of potential. As a result of these problems, aqueous sodium-ion batteries have grown in popularity in recent years [6], [7], [8], [9]. Table 2.1 shows some recent cathode material used in aqueous sodium ion battery.

Table 2.1 Recent cathode materials used for aqueous sodium ion battery.

Sr. No.	Material	Electrolyte	Discharge Capacity / Rate	Retention Capacity (%)	Cycles	Ref.
1	NiHCF	1 M NaNO ₃	76 mAh g ⁻¹ @ 1 C	93	1000	[11]
2	Na _{0.44} MnO ₂	6 M NaNO ₃	123.5 mAh g ⁻¹ @1 A g ⁻¹			[8]
3	Na ₂ VTi-(PO ₄) ₃ @C	5 M NaClO ₄	52.4 mAh g ⁻¹ @ 1C			[12]
4	Na _{0.44} MnO ₂ - CNT	1 M Na ₂ SO ₄	70 mAh g ⁻¹ @ 50 mA g ⁻¹	53.1	300	[13]
5	Na _{0.57} CoO ₂	0.5 M Na ₂ SO ₄	57 mAh g ⁻¹ @ 0.7C	79	1000	[14]
6	Na ₃ MnCO ₃ PO ₄	5 M NaNO ₃	77.05 mAh g ⁻¹ @ 0.2 C	89	50	[15]

2.2 Transition Metal Fluorides

Polyanion compounds and layered type oxides NaMO₂ (M = V, Cr, Mn, Fe, Co, and Ni) have been the most researched cathode materials for sodium-ion batteries. However, due to their inherently low electrical conductivities, metal fluoride cathodes have received little attention. Metal fluorides have a greater oxidative stability than layered typed oxides, which can have problems with oxygen release. They also have high electrode potentials, comparable to polyanionic compounds. Fluoride-based materials have a greater specific capacity and specific energy than non-fluoride-based materials due to high electronegativity. Metal fluorides are electrical insulators, although this can be mitigated with the use of conductive coatings or additives. As a result, certain transition metal fluorides have open structures with strong interstitial site coordination, making them ideal for tolerating Na⁺ (but not always Li⁺ ions). Sodium insertion/de-insertion is possible with various groups of sodium-containing metal fluorides. Sodium fluoroperovskites, or NaMF₃, are a divalent transition metal family that includes Mg, Mn, Fe, Co, Ni, Cu, and Zn [16], [17]. The structure of

NaMF_3 is perovskite, which exhibits intrinsic 3D diffusion channels which favours very efficient electron and ion transport, metal-fluoride bonding elevates the redox potential which ultimately increase the energy density [18] [19]. Herein this study we are focusing on the synthesis, characterization and electrochemical performance of Sodium Nickel Fluoride (NaNiF_3).

2.3 Sodium Nickel Fluoride

2.3.1 Synthesis methods

There are very limited methods are reported for the synthesis of NaNiF_3 , synthesis of NaNiF_3 has been very difficult due to involvement of highly toxic material and dangerous techniques. In one study, sodium nickel fluoride was synthesised in a one-step solvothermal process by stirring NH_4F , $\text{NiCl}_2 \cdot 6\text{H}_2\text{O}$ and sodium citrate dihydrate in a mixed solvent of ethylene glycol and water (18:1) for 1 hour, then Heating in teflon autoclave at 200°C for 24 hours. [18].

As an alternative to the dangerous high-pressure fluorination approach a study reports the mechano-chemical reaction involved as a nonconventional solid-state process for large-scale production of fluoride materials. Mechanical grinding of NaF with binary metal fluorides (NiF_2) for various lengths of time under Ar atmosphere produced Sodium Nickel fluoroperovskites [20].

In a study reported sodium nickel fluoride composite with nickel was made using a simple electrochemical corrosion technique in which 0.25 g NaF was dissolved in 30 ml distilled water, followed by 0.6 ml H_2O_2 and 0.3 ml HCl . The homogenous solution was transferred into a 50 ml Teflon lined autoclave after 20 minutes of stirring, and Ni foams were then inserted in the autoclave, 80 percent of its volume was filled with distilled water. After that, the autoclave was sealed and cooked in an oven for 24 hours at 160°C [21].

sodium nickel fluoride with a novel hydrated sodium nickel composition using an aqueous solution method, $\text{NaNiF}_3 \cdot 3\text{H}_2\text{O}$ was synthesised and reported in research done at room temperature. There were 1.7135 g of NiCl_2 dissolved in 25mL of pure water. We next added NaF (0.9g) until we had a perfect mixture. It was then heated to 60°C to partially evaporate the solvent, which resulted in a light green powder after 6 hours of stirring. Using distilled water, the precipitate was washed and dried at 60

degrees Celsius. The NaNiF_3 perovskite phase was not produced during the precipitation procedure [17].

In a study microwave assisted technique employed by using in situ template technique to make hollow sodium nickel fluoride nano-cubes placed on multiwall carbon nanotubes (SNF–MWCNT). The catalysts were synthesised with the help of ionic liquid (IL). Ionic Liquid was employed to functionalize MWCNTs as well as a fluorine source in the production of hollow NaNiF_3 NT, and their electrochemical efficacy in the electro-oxidation of urea was studied [22].

A study conducted reports the synthesis of sodium transition metal by roll quenching method, extremely crystalline NaFeF_3 crystals were produced. NaFeF_3 was made of NaHF_a and FeF_2 with molar ratio of 1:1. In a glove box Filled with Ar, the mixture was crushed and put in a silica coated Pt tube coated. A few mm diameter hole at the bottom of the Pt and silica tubes allows the melted sample to be injected into a single copper roller. The powder sample in the roll-quench machine was heated using the joule heat of induction current in a Pt tube, with high pressure Ar gas the molten liquid was injected and quenched on a single rotating copper roller after being heated over 1000 C for 40 seconds, quenched flake-like sample was created [23].

In a study, they developed a microwave-assisted solvothermal method for the facile synthesis of various Na_xMF_y nano powders (sodium cobalt fluoride (NaCoF_3), sodium manganese fluoride (NaMnF_3), and sodium iron fluoride (Na_3FeF_6) using low-cost precursors under air atmosphere [24].

2.3.2 Electrochemical Performance

The mechanochemically synthesised NaNiF_3 has a poor cycling stability and a practical discharge capacity of 40 mAh g^{-1} . The low capacity of such materials may be attributed to poor electrical conductivity caused by the wide band gap generated by the Mn–F and Ni–F bonds, as well as cut-off voltage restrictions of up to 4V to prevent electrolyte dissolution, this might explains that why we don't get a lot of capacity out of NaNiF_3/Na cells due to their low charge [20].

In a study with a charge and discharge capacity at rate of 0.07 mA cm^{-2} was found to be 197 mAh g^{-1} inbetween voltage window of 1.5 V and 4.5 V, 100 percent columbic efficiency was attained for NaFeF_3 [23].

The electrochemical performance of the synthesized NaNiF_3/Ni composite as anode for lithium-ion batteries was investigated using a standard charge/ discharge test, which revealed apparent voltage plateaus, indicating that NaNiF_3 may be used in lithium-ion batteries. As the cycle number increases, the discharge and charge capacities drop, eventually stabilising at 0.12 mAh cm^{-2} after 100 cycles [21].

The $\text{NaNiF}_3\text{-MWCNT}$ due to rich in Ni^{3+} surface, the electro catalyst achieved a high current density of $3.1 \text{ A cm}^{-2} \text{ mg}^{-1}$ in 5 M KOH and 0.3 M urea at 20 mV s^{-1} . For urea oxidation, the catalytic activity of $\text{NaNiF}_3\text{-MWCNT}$ was found to be superior to a commercially available Ni-C catalyst. Using sodium nickel fluoride-MWCNT IL as an anode catalyst and a small amount of loading, the direct urea/air unit fuel cell displayed extraordinarily promising performance [22].

In a study NaFeF_3 shows rechargeable capacity of 169 mAh g^{-1} and an energy density of over 500 Wh kg^{-1} , making it the most energy dense iron-based material for sodium-ion battery cathode ever recorded.[25]

In a study high capacity and stability achieved using FeF_2 nanoparticles Composite with reduced graphene oxide electrode. The electrode has outstanding cycling stability and a high capacity of 175 mAh g^{-1} at 0.2 A g^{-1} . It also has a high-rate capability of 78 mAh g^{-1} at 10 A g^{-1} [26].

The hollow spheres of perovskite fluoride (NaNiF_3) employed as supercapacitor electrodes in a study possessed a high specific capacitance $\sim 1300 \text{ F g}^{-1}$ at 5 A g^{-1} , as well as good rate performance, and extended cycle stability (more than 90 percent capacity retention after 8000 cycles). With a power density of 1.65 kW kg^{-1} and Energy density is 51.78 Wh kg^{-1} [18].

Summary:

This chapter consists of literature review on aqueous sodium ion battery and Recent cathode materials utilised in aqueous sodium ion battery applications. In addition, different synthesis methods and electrochemical performance of transition metal fluoride (Sodium Nickel Fluoride) for different electrochemical applications is discussed in this chapter.

References:

- [1] B. Cho, H. Lim, H. N. Lee, Y. M. Park, H. Kim, and H. J. Kim, "High-capacity and cycling-stable polypyrrole-coated MWCNT@polyimide core-shell nanowire anode for aqueous rechargeable sodium-ion battery," *Surf. Coatings Technol.*, vol. 407, no. January, p. 126797, 2021.
- [2] J. Chen *et al.*, "High-energy-density aqueous sodium-ion batteries enabled by chromium hexacyanochromate anodes," *Chem. Eng. J.*, vol. 415, no. January, p. 129003, 2021.
- [3] D. Bin *et al.*, "Progress in Aqueous Rechargeable Sodium-Ion Batteries," *Adv. Energy Mater.*, vol. 8, no. 17, pp. 1–31, 2018.
- [4] D. Choi, S. Lim, and D. Han, "Advanced metal–organic frameworks for aqueous sodium-ion rechargeable batteries," *J. Energy Chem.*, vol. 53, pp. 396–406, 2021.
- [5] A. C. Nwanya, M. M. Ndipingwi, O. Anthony, F. I. Ezema, M. Maaza, and E. I. Iwuoha, "Impedance studies of biosynthesized Na_{0.8}Ni_{0.33}Co_{0.33}Mn_{0.33}O₂ applied in an aqueous sodium-ion battery," *Int. J. Energy Res.*, vol. 45, no. 7, pp. 11123–11134, 2021.
- [6] F. Gu, T. Sun, X. Yao, M. Shui, and J. Shu, "Studies on the improved electrochemical performance and the sodium ion migration mechanism of Na_{0.44}MnO₂-CNT electrodes for aqueous sodium batteries," *J. Phys. Chem. Solids*, vol. 149, no. October 2020, p. 109771, 2021.
- [7] M. Liu *et al.*, "Aqueous rechargeable sodium ion batteries: developments and prospects," *Mater. Today Energy*, vol. 17, 2020.
- [8] L. Rakočević, S. Štrbac, J. Potočnik, M. Popović, D. Jugović, and I. S. Simatović, "The Na_xMnO₂ materials prepared by a glycine-nitrate method as advanced cathode materials for aqueous sodium-ion rechargeable batteries," *Ceram. Int.*, vol. 47, no. 4, pp. 4595–4603, 2021.
- [9] T. Jin *et al.*, "High-Energy Aqueous Sodium-Ion Batteries," *Angew. Chemie - Int. Ed.*, vol. 60, no. 21, pp. 11943–11948, 2021.

- [10] R. R. Salunkhe, Y. V. Kaneti, and Y. Yamauchi, "Metal-Organic Framework-Derived Nanoporous Metal Oxides toward Supercapacitor Applications: Progress and Prospects," *ACS Nano*, vol. 11, no. 6, pp. 5293–5308, 2017.
- [11] S. Park, J. Kim, S. H. Yi, and S. E. Chun, "Coprecipitation Temperature Effects of Morphology-Controlled Nickel Hexacyanoferrate on the Electrochemical Performance in Aqueous Sodium-Ion Batteries," *ChemSusChem*, vol. 14, no. 4, pp. 1082–1093, 2021.
- [12] L. Shen *et al.*, "NASICON-Structured Na₂VTi(PO₄)₃@C for Symmetric Aqueous Rechargeable Na-Ion Batteries with Long Lifespan," *ACS Sustain. Chem. Eng.*, vol. 9, no. 9, pp. 3490–3497, 2021.
- [13] F. Gu, T. Sun, X. Yao, M. Shui, and J. Shu, "Studies on the improved electrochemical performance and the sodium ion migration mechanism of Na_{0.44}MnO₂-CNT electrodes for aqueous sodium batteries," *J. Phys. Chem. Solids*, vol. 149, no. July 2020, p. 109771, 2021.
- [14] A. C. Nwanya, M. M. Ndipingwi, F. I. Ezema, E. I. Iwuoha, and M. Maaza, "Bio-synthesized P2-Na_{0.57}CoO₂ nanoparticles as cathode for aqueous sodium ion battery," *J. Electroanal. Chem.*, vol. 878, p. 114600, 2020.
- [15] K. Shiprath, H. Manjunatha, K. C. Babu Naidu, A. Khan, A. M. Asiri, and R. Boddula, "Na₃MnPO₄CO₃ as cathode for aqueous sodium ion batteries: Synthesis and electrochemical characterization," *Mater. Chem. Phys.*, vol. 248, no. March, p. 122952, 2020.
- [16] H. Euchner and O. Clemens, "Unlocking the potential of weberite-type metal fluorides in electrochemical energy storage," *npj Comput. Mater.*, no. October 2018, pp. 1–10, 2019.
- [17] E. C. Gonzalo, M. Hoelzel, M. T. Azcondo, U. Amador, F. Garc, and A. Kuhn, "Synthesis and Characterization of NaNiF₃ · 3H₂O: An Unusual Ordered Variant of the ReO₃ Type," 2015.
- [18] N. Hussain, F. Wu, W. Younas, and L. Xu, "Hollow sphere formation by the self aggregation of perovskite fluoride NaNiF₃ nanocrystals and the application of these spheres as an electrode in an ultrahigh performance asymmetric

- supercapacitor,” *New J. Chem.*, vol. 43, no. 30, pp. 11959–11967, 2019.
- [19] N. Dimov, A. Nishimura, K. Chihara, A. Kitajou, I. D. Gocheva, and S. Okada, “Transition metal NaMF₃ compounds as model systems for studying the feasibility of ternary Li-M-F and Na-M-F single phases as cathodes for lithium-ion and sodium-ion batteries,” *Electrochim. Acta*, vol. 110, pp. 214–220, 2013.
- [20] I. D. Gocheva, M. Nishijima, T. Doi, S. Okada, J. Yamaki, and T. Nishida, “Mechanochemical synthesis of NaMF₃ (M = Fe , Mn , Ni) and their electrochemical properties as positive electrode materials for sodium batteries,” vol. 187, pp. 247–252, 2009.
- [21] S. Ni, J. Ma, X. Lv, X. Yang, and L. Zhang, “Fabrication of NaNiF₃/Ni composite and its application in lithium ion batteries,” *Mater. Lett.*, vol. 124, pp. 264–266, 2014.
- [22] N. Kakati, J. Maiti, K. S. Lee, B. Viswanathan, and Y. S. Yoon, “Hollow Sodium Nickel Fluoride Nanocubes Deposited MWCNT as An Efficient Electrocatalyst for Urea Oxidation,” *Electrochim. Acta*, vol. 240, pp. 175–185, 2017.
- [23] A. Kitajou, H. Komatsu, K. Chihara, I. D. Gocheva, S. Okada, and J. Yamaki, “Novel synthesis and electrochemical properties of perovskite-type NaFeF₃ for a sodium-ion battery,” *J. Power Sources*, vol. 198, pp. 389–392, 2012.
- [24] J. Hwang and J. Chun, “Microwave-assisted solvothermal synthesis of sodium metal fluoride (Na_xMF_y) nanopowders,” *J. Am. Ceram. Soc.*, vol. 102, no. 11, pp. 6475–6479, 2019.
- [25] A. Kitajou, Y. Ishado, T. Yamashita, H. Momida, T. Oguchi, and S. Okada, “Cathode Properties of Perovskite-type NaMF₃ (M = Fe, Mn, and Co) Prepared by Mechanical Ball Milling for Sodium-ion Battery,” *Electrochim. Acta*, vol. 245, pp. 424–429, 2017.
- [26] D. Ni *et al.*, “Improved rate and cycling performance of FeF₂-rGO hybrid cathode with poly (acrylic acid) binder for sodium ion batteries,” *J. Power Sources*, vol. 413, no. September 2018, pp. 449–458, 2019.

CHAPTER 3

EXPERIMENTATION AND CHARACTERIZATION

3.1 Synthesis Method

3.1.1 Precipitation Route

Precipitation method also known as "wet precipitation," "chemical precipitation," or "aqueous precipitation" [1]. Precipitation is the process of transforming a liquid into a solid (It's not always crystalline; it could possibly be amorphous) by converting the solution into an insoluble form or supersaturating the solution. It entails adding chemical reagents to the solution and then separating the precipitates from it. It is a very useful technique since it is a single-step procedure that aids in large-scale manufacture of material free of contaminants [2]. The kind and concentration of ionic metals present in solution, the precipitant utilized, the reaction conditions, and the presence of other elements that may limit the precipitation reaction are all factors that influence the effectiveness of a precipitation process [3]. Precipitation is mostly used to remove impurities, separate materials, and prepare raw materials [4].

3.1.2 Hydrothermal Route

The method of hydrothermal synthesis is increasingly being used in materials research and solid-state chemistry. Hydrothermal reactions are commonly used for compound synthesis or stabilization, single crystal growth, finely divided materials fabrication, and micro crystallites with well-defined size and morphology[5]. Hydrothermal synthesis is a chemical reaction in which materials that are relatively insoluble under normal conditions are dissolved and recrystallized in the closed system in the presence of aqueous solvents at pressures more than 1 atm and temperatures greater than 100°C. Steel autoclave with teflon vessels (23 ml) inside, hydrothermal reactions take place between 100 and 250°C, as teflon is a non-reactive substance, it does not react with the initial components. In hydrothermal synthesis, water is used as a catalyst or as a component of the solid phases. Because hydrothermal synthesis takes

place in a closed vessel, the temperature and degree of filling dictate the pressure. [6]. Fig. 3.1 shows the autoclave used for hydrothermal process.



Figure 3.1 Autoclave used for the hydrothermal synthesis technique.

3.2 Material Characterization Techniques

3.2.1 X-Ray Diffraction

X-ray diffraction is a non-destructive analytical technique for evaluating materials' chemical and physical qualities. In all sectors of science and technology, it is widely used. Some of the uses of this technology include crystalline sized, crystallographic sized, unit cell structure, crystal structure, phase analysis, macrostrain and macro stress. The most common use of the X-ray diffraction method is to identify crystalline phases or molecules qualitatively [7]. In this technique a monochromatic X-ray beam is used to examine the substance under consideration. When the incident beam collides with the material, the substance's atoms scatter the X-rays, causing both constructive and destructive interference. The diffraction of X-rays is described by Bragg's Law which is as follow;

$$n\lambda = 2d\sin\theta \dots\dots\dots (1)$$

The shape and size of the material's unit cell confirm the direction of diffractions, while the intensity of diffracted X-rays is determined by the arrangement of atoms in the material. Because most materials are not single crystals in nature, the X-ray beam

will consider all interatomic sites and will detect all possible diffraction peaks at a specific angle [8]. Fig. 3.2 depicts the XRD process schematically.

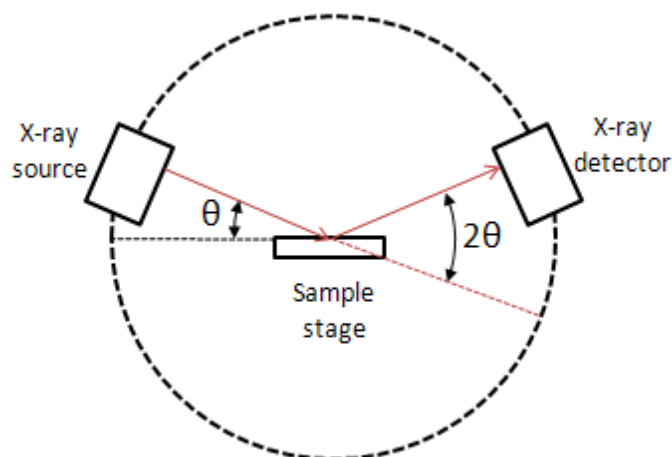


Figure 3.2 Schematic of X-Rays diffraction Process.

3.2.2 Scanning Electron Microscopy

On a nanoscale (nm) to micrometer (μm) scale, scanning electron microscopy (SEM) can be utilized to investigate and characterize heterogeneous organic and inorganic materials. The lens system, electron gun, electron collector, visual and photorecording cathode ray tubes (CRTs), and associated electronics are the core components of the SEM. The electrons beam falls across the surface of the material in this procedure. The surface topography of materials such as catalysts, polymers, and crystals are then determined by detecting electrons reflected by the sample's surface as well as emitted secondary electrons. Particle size, magnetic domains, crystal shape, and surface flaws are all examined using this method [9],[10]. The design and function of SEM and EPMA are quite similar and the two devices have a lot in common in terms of capabilities. Fig. 3.3 schematic mechanism of scanning electron microscopy.

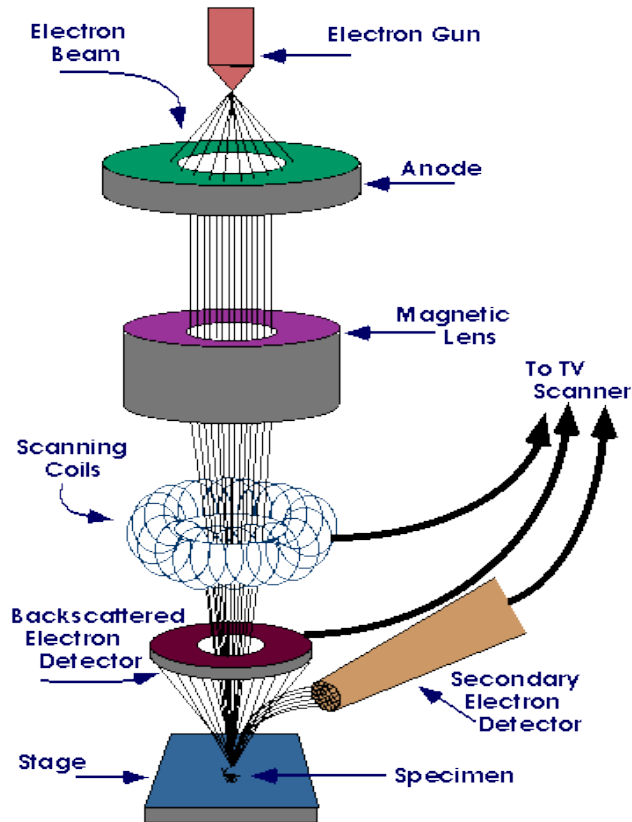


Figure 3.3 Schematic drawing of the scanning electron microscopy.

3.2.3 Energy Dispersive X-Ray Spectroscopy

EDS is a sort of elemental analysis that counts how many distinct elements are present in a sample. This method provides the number of substances at a given location but not the total quantity of each element. It's frequently used in conjunction with SEM or TEM to provide a nanoscale image of particles. Fig. 3.4 schematic mechanism of EDX.

Energy dispersive spectroscopy became a commercial product in the early 1970s, and it quickly overtook WDS in popularity. Because there are no moving parts in the EDS like the rotation detector in the WDS, the overall structure is fairly basic [11]. The detector collects X-ray signals from all ranges of elements in a sample at once, rather than collecting X-ray signals one by one, which makes EDS devices comparatively rapid. Energy dispersion resolution is typically around 150–200 eV, which is lower than WDS resolution. O ($Z=8$) is the lightest element that can be detected, not C ($Z=6$). However, key advantages like as inexpensive cost and quick analysis make these drawbacks minor [12]. The EDS spectrum is a graph that shows

the relationship between the intensity of X-rays and their respective energies. In a spectrum ranging from 0.1 to around 10–20 keV, both light and heavy elements can be seen.

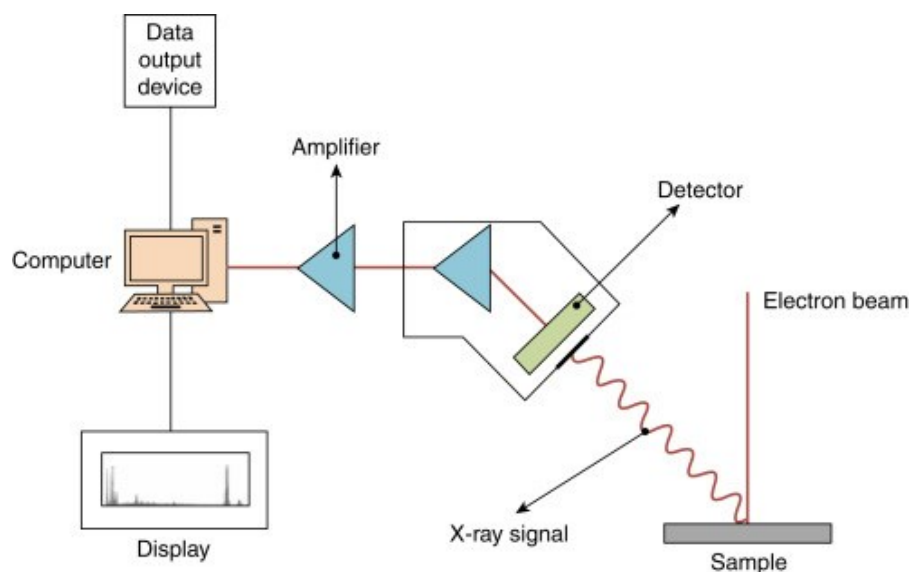


Figure 3.4 Schematic mechanism of energy dispersive X-Ray spectroscopy.

3.2.4 Thermogravimetric Analysis

Thermogravimetric analysis (TGA) is an analytical technique that monitors the weight change that occurs as a sample is heated at a constant pace to assess a material's thermal stability and fraction of volatile components. Thermal stability, volatile content, moisture, organic linker in a sample, and the percent composition of components in a compound are some of the most common applications of this characterization approach [13]. Fig. 3.5 shows schematic mechanism of TGA.

The basic principle is that in a certain gas environment, such as Ar, air, or another gas, the temperature is progressively increased from zero to the appropriate ultimate temperature. When the temperature in the sample rises, the contents begin to evaporate. Moisture is commonly the first material to be removed from a sample, resulting in a change in mass, this mass is measured on the weight balance continuously during the process which is placed outside the furnace [14]. Other volatile substances, such as organic residue, begin to escape after moisture. The temperature at which the material begins to breakdown, which is the primary point on the curve, can be used to determine the sample's stability. Following that, the line abruptly dips, resulting in a significant material loss. This temperature is known as the

decomposition temperature, and it determines the material's stability [15]. The weight of the material is plotted versus temperature or time to show thermal changes in the sample, such as solvent loss, water loss, and hydration loss. The final mass residue is observed at the end of the process, and the overall mass loss is calculated.

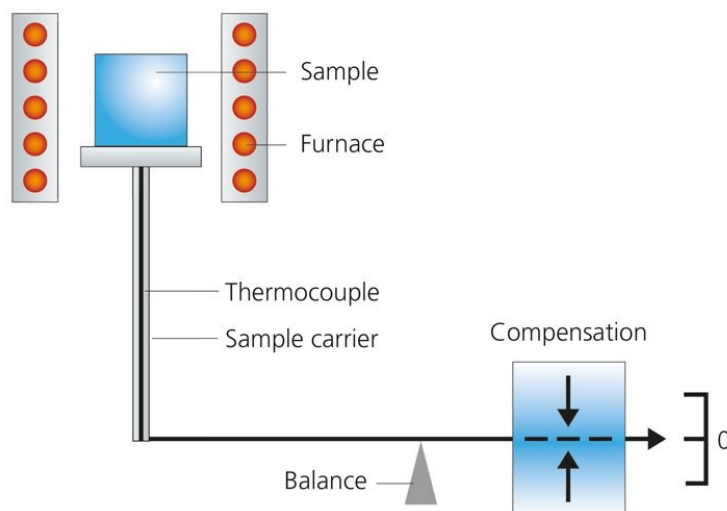


Figure 3.5 Schematic of TGA.

3.2.5 BET

The Brunauer–Emmett–Teller (BET) theory attempts to explain the physical adsorption of gas molecules on a solid surface and serves as the basis for a critical analytical approach for measuring material specific surface area. The phenomenon is referred to as physical adsorption, or physisorption. Nitrogen is commonly utilized in BET surface area analysis because it is available in high purity and has a strong interaction with most materials. The sample compartment is then gradually filled with known amounts of nitrogen gas. Partially vacuum conditions were used to achieve relative pressures lower than atmospheric pressure. There is no additional adsorption after the saturation pressure is reached, regardless of how high the pressure is raised. Pressure transducers with high precision and accuracy detect pressure changes caused by the adsorption process. After the adsorption layers have developed, the sample is taken out of the nitrogen atmosphere and heated, causing the adsorbed nitrogen to be released and quantified [16]. The information gathered is plotted as a BET isotherm,

which shows the amount of gas adsorbed as a function of relative pressure. Fig. 3.5 shows the schematic mechanism of BET.

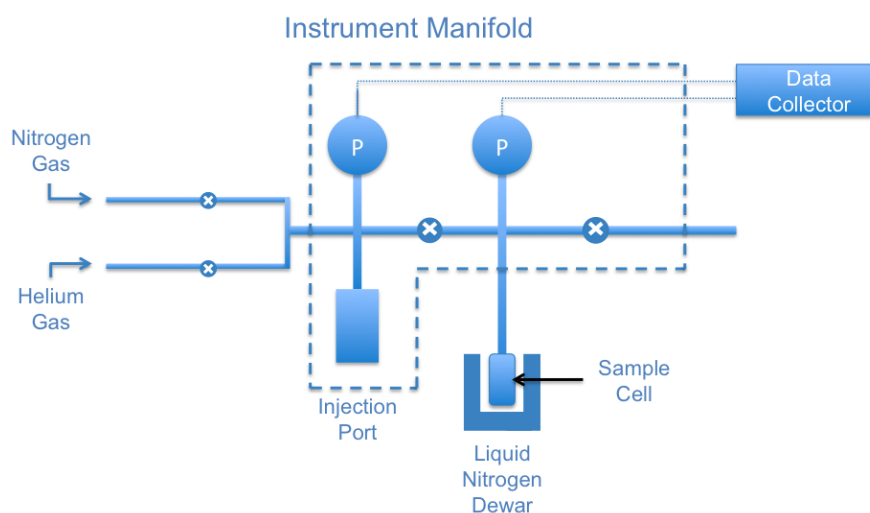


Figure 3.6 Schematic mechanism of BET.

3.3 Electrochemical Characterization

3.3.1 Suspension formation & Electrolyte

Working electrode deposit suspension was made by adding 2 mg of active material in 80 μl of ethanol for dispersion and 20 μl Nafion as a binder, after which it is ultrasonicated for 1 hour at temperature $\pm 35^\circ\text{C}$ for perfect dispersion, then deposited on polished glassy carbon electrode for electrochemical measurements. 1 M Na_2SO_4 is used as an electrolyte for electrochemical measurements.

Electrochemical Workstation

For electrochemical characterization, electrochemical workstation CHI 760E (CH Instruments, Texas, USA) based on a three-electrode system is used, which include platinum wire as a counter electrode, Ag/AgCl as reference electrode, and

glassy carbon electrode as working electrode. Following Electrochemical Techniques are used for electrochemical Characterization.

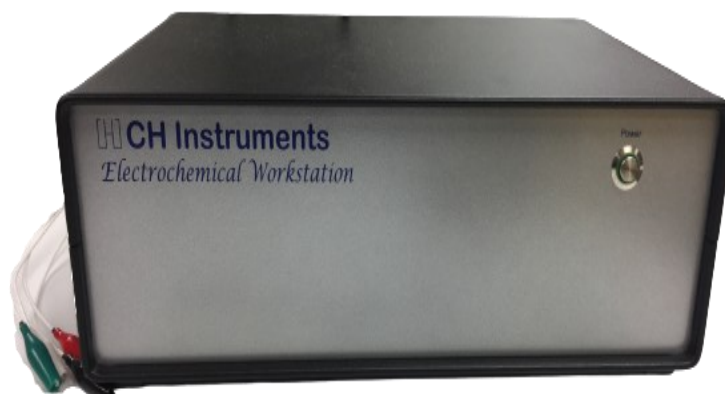


Figure 3.7 Electrochemical Workstation.

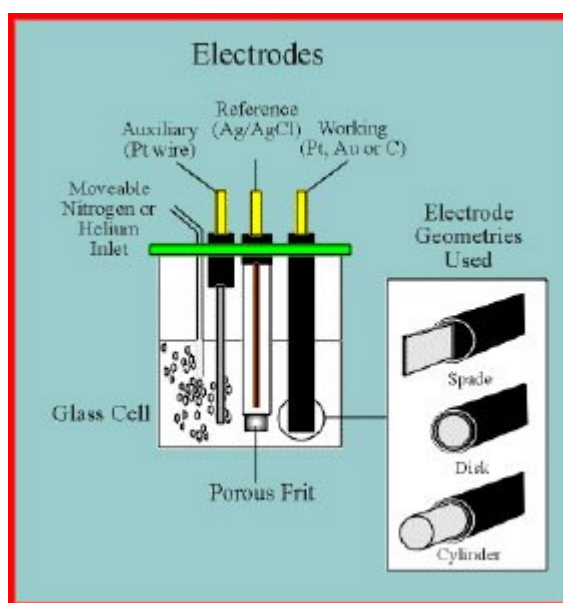


Figure 3.8 3 Electrode System Configuration (Retrieved from Electrochemical cell and electrodes for cyclic voltammetry, Demonstration by Dr. Alf Bacher; notes by Shadi Rezai)

3.3.2 Cyclic Voltammetry (CV)

As far as electrochemical material testing goes, CV is the most basic. This is done by moving the potential between the defined bounds, and then recording the current as a result (from positive to negative, and vice versa-). As a result of the information gathered by CV, we can better comprehend the material's electrochemical

properties. To anticipate an electrode's capacitive behavior, the redox peak, or reduction and oxidation peak, is determined via visual interpretation of the electrode's cyclic voltammogram. As a result, the material's oxidation and reduction potential may be evaluated.

There is a ramp signal that is fed into the CV. In order to flip the nature of a cyclic voltammogram, a positive ramp (with a positive slope) signal is used for the forward scan, while the voltage is switched after the first half-cycle. To achieve equilibrium, the system must go back to where it came from, which is where redox reactions take place. In a cycle, it gives information on the system's evolution. By carefully examining the CV curve, many significant conclusions may be drawn about the material and its characteristics. (For example, capacitive nature, etc.) as well as the system's behavior (does it have irreversible, reversible, or semi-reversible nature). A single potential cycle or numerous potential cycles might be used in the CV experiment. The scan rate is defined as the slope of the ramp signal in volts per unit time [17].

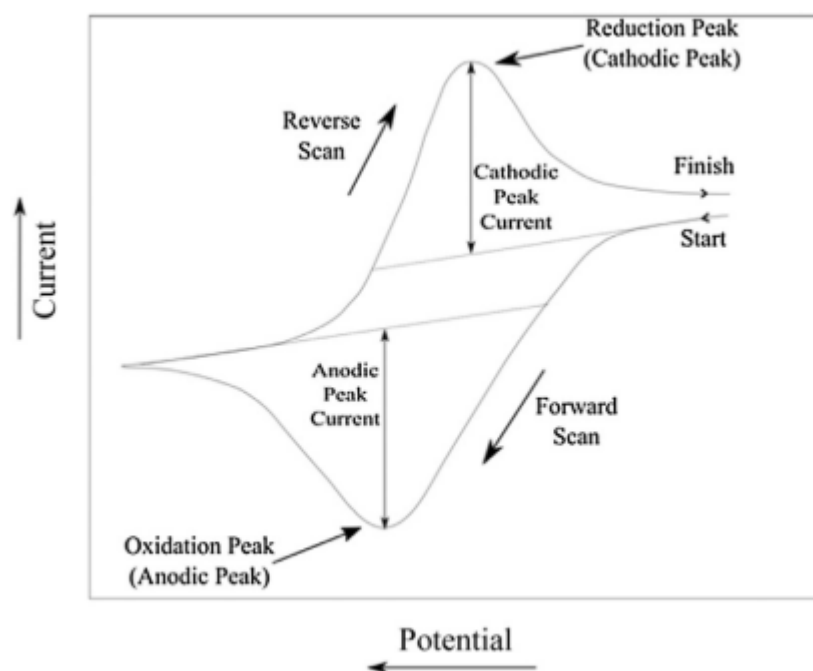


Figure 3.9 Cyclic Voltammetry [17].

3.3.3 Chronopotentiometry (CP)

Chronopotentiometry (CP) studies the behavior of material by varying potential with time, where chrono denotes time and poten denotes potential. The potential of an electrode changes when electricity is introduced to it at first. The chrono-potentiometric response is calculated by recording this change over time and plotting it. Characterizing electrode reactions using CP is possible. The electrochemical characteristics of insertion materials may be characterized using chrono-potentiometric methods. The gravimetric charge discharge test is used to assess a material's durability or an electrochemical cell's stability. Simply test is repeated for thousands of cycles at a certian current density ($A\ g^{-1}$) within a Specific potential window. It's a charge discharge cycle for each cycle. The purpose of the test is to determine cycling stability, which validates a material's stability through a high number of cycles. Numerous variables might be influenced by the charging and discharging pace of a cell phone. Numerous characteristics, like as capacitance, has impact on capacity by high charging or drainage rates. High-speed charging reduces the device's capacitance value, which in turn reduces its energy density. For the same capacitance values, galvanostatic cycling and CV techniques are superior to a faster charging rate [17].

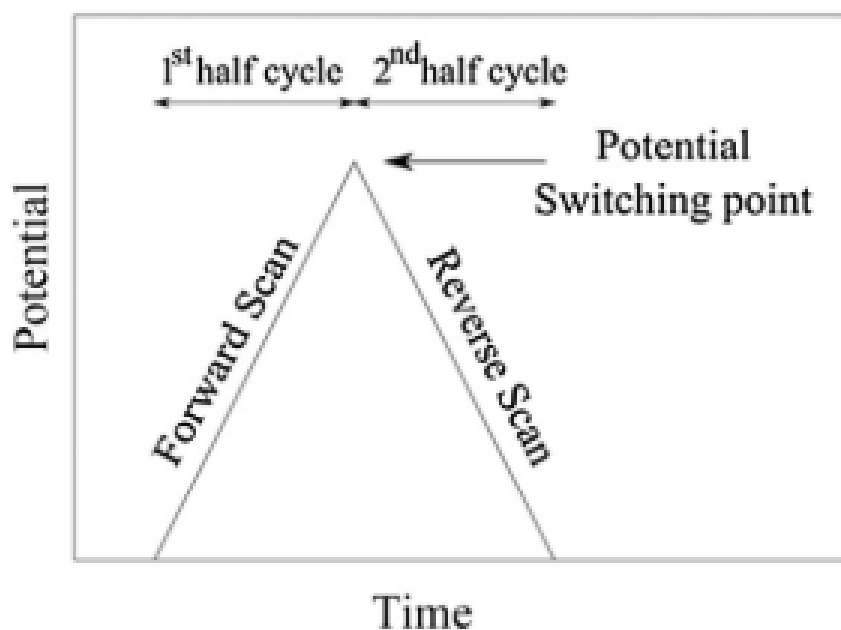


Figure 3.10 Chrono-potentiometry [17].

3.3.4 Electrochemical Impedance Spectroscopy

An electrochemical cell's impedance is determined using EIS. With the use of a tiny sinusoidal (AC) voltage, one may estimate the impedance of an electrode by measuring the current produced by the electrode in proportion to the sinusoidal voltage. Ohm's law is then used to compute the impedance of the circuit. EIS technique is based in this mechanism. Because impedance is a function of frequency, it is required to investigate the various frequency ranges in order to obtain an impedance spectrum. EIS tests are carried out in a certain frequency domain with signal parameters such as rms signal amplitude perturbation and data recording speeds being examined. The AC voltage signal should be delivered in the right frequency range for EIS analysis (at the room temperature). When comparing the impedance spectra produced from the EIS experiment to a modified Randles circuit, it is possible to gain a better understanding.

According to an EIS's Nyquist plot, real and imaginary parts are related to each other in impedance. In the Nyquist plots, high frequency and low frequency are separated. That semicircular shape is due to the charge transfer resistance RCT, which is present at the electrode/electrolyte interface. Because of Warburg impedance, the low-frequency EIS spectra have a straight-line (constant slope) characteristic (Z_w). When it comes to polarization resistance, it's the total of $R_{ct} + Z_w$. For a given impedance, the Nyquist plot is produced on both the real and imaginary axes (on the real axis, the imaginary component of the impedance becomes zero) [17].

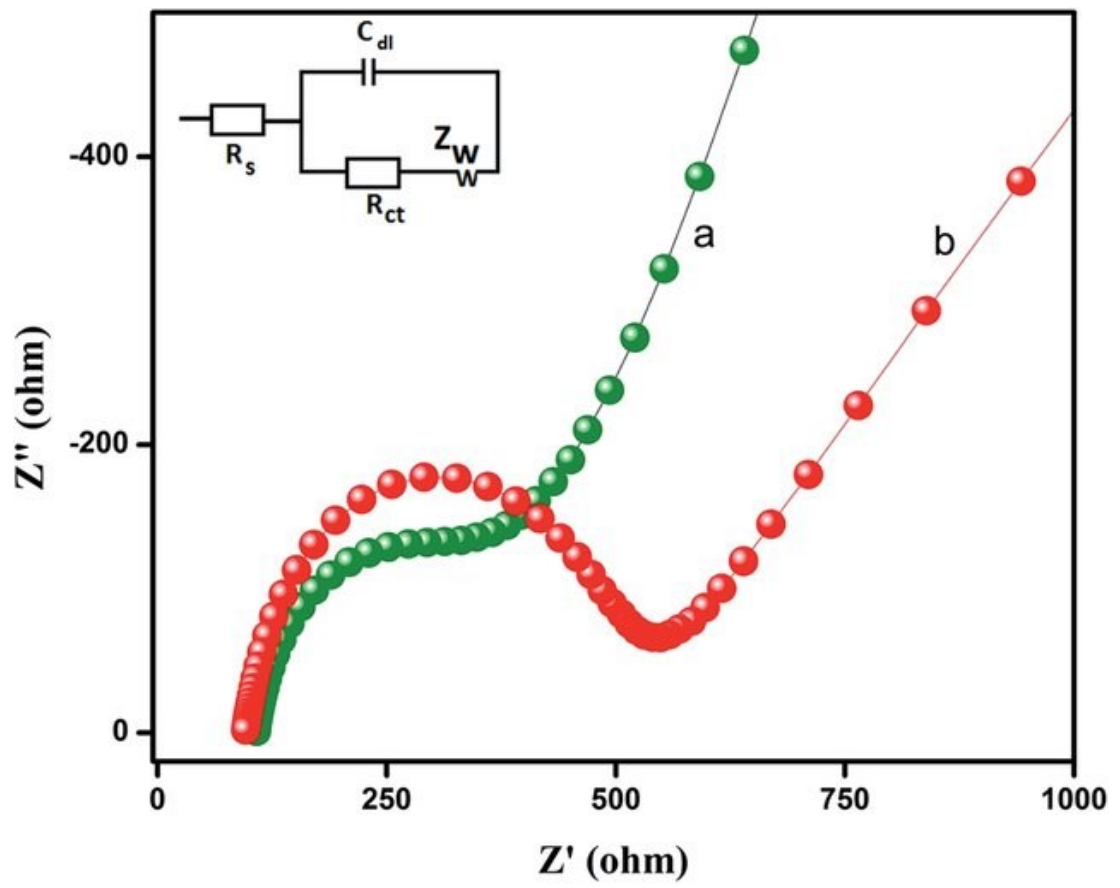


Figure 3.11 Electrochemical Impedance Spectroscopy [17].

Summary:

In this chapter initially different chemical synthesis techniques are discussed including Precipitation method and hydrothermal method, followed by the material characterization including brief introductions to XRD, SEM, EDS, TGA, BET. In addition, electrode material suspension recipe electrochemical workstation specifications and all electrochemical characterization techniques used for electrode characterization are discussed.

References

- [1] S. Mazumder, A. K. Nayak, T. J. Ara, and M. S. Hasnain, *Hydroxyapatite composites for dentistry*. Elsevier Inc., 2018.
- [2] G. Sharma *et al.*, “Novel development of nanoparticles to bimetallic nanoparticles and their composites: A review,” *J. King Saud Univ. - Sci.*, vol. 31, no. 2, pp. 257–269, 2019.
- [3] Y. Dahman, “Nanopolymers**By Yaser Dahman, Kevin Deonanan, Timothy Dontosos, and Andrew Iammateo.,” *Nanotechnol. Funct. Mater. Eng.*, pp. 121–144, 2017.
- [4] Y. Ma, M. Svärd, X. Xiao, J. M. Gardner, R. T. Olsson, and K. Forsberg, “Precipitation and crystallization used in the production of metal salts for li-ion battery materials: A review,” *Metals (Basel)*., vol. 10, no. 12, pp. 1–16, 2020.
- [5] R. Piticescu, A. M. Motoc, A. I. Tudor, C. F. Rusti, R. M. Piticescu, and M. D. Ramiro-sanchez, “Hydrothermal Synthesis of Nanostructured Materials for Energy Harvesting Hydrothermal Synthesis of Nanostructured Materials for Energy Harvesting Applications 1 . Thermodynamic and Kinetic Approaches in Hydrothermal Synthesis of Nanomaterials,” no. September, 2015.
- [6] Ö. Ece, “Hydrothermal Synthesis And Structural Characterization Of Open-Framework Metal Phosphates Templated With Organic Diamines,” no. July, p. 71, 2012.
- [7] A. V. Llewellyn, A. Matruglio, D. J. L. Brett, R. Jervis, and P. R. Shearing, “Using in-situ laboratory and synchrotron-based x-ray diffraction for lithium-ion batteries characterization: A review on recent developments,” *Condens. Matter*, vol. 5, no. 4, pp. 1–28, 2020.
- [8] S. I. AL-Saedi, A. J. Haider, A. N. Naje, and N. Bassil, “Improvement of Li-ion batteries energy storage by graphene additive,” *Energy Reports*, no. September, 2019.
- [9] Y. Yuan, K. Amine, J. Lu, and R. Shahbazian-Yassar, “Understanding materials challenges for rechargeable ion batteries with in situ transmission electron microscopy,” *Nat. Commun.*, vol. 8, no. May, pp. 1–14, 2017.

- [10] I. R. Mattson, “Stability of the Graphite Electrode for Li-ion Batteries,” no. July, p. 85, 2013.
- [11] Z. M. Wang, J. Wagner, S. Ghosal, G. Bedi, and S. Wall, “SEM/EDS and optical microscopy analyses of microplastics in ocean trawl and fish guts,” *Sci. Total Environ.*, vol. 603–604, pp. 616–626, 2017.
- [12] F. Georget, W. Wilson, and K. L. Scrivener, “edxia: Microstructure characterisation from quantified SEM-EDS hypermaps,” *Cem. Concr. Res.*, vol. 141, no. October 2020, p. 106327, 2021.
- [13] K. R. Rajisha, B. Deepa, L. A. Pothan, and S. Thomas, “Thermomechanical and spectroscopic characterization of natural fibre composites,” *Interface Eng. Nat. Fibre Compos. Maximum Perform.*, pp. 241–274, 2011.
- [14] N. Saadatkah *et al.*, “Experimental methods in chemical engineering: Thermogravimetric analysis—TGA,” *Can. J. Chem. Eng.*, vol. 98, no. 1, pp. 34–43, 2020.
- [15] Y. Huang *et al.*, “Thermal Stability and Reactivity of Cathode Materials for Li-Ion Batteries,” *ACS Appl. Mater. Interfaces*, vol. 8, no. 11, pp. 7013–7021, 2016.
- [16] P. M. V. Raja and A. R. Barron, “2.3: BET Surface Area Analysis of Nanoparticles,” *Phys. Methods Chem. Nano Sci.*, vol. i, pp. 1–7, 2019.
- [17] Y. S. Choudhary, L. Jothi, and G. Nageswaran, *Electrochemical Characterization*, vol. 2. Elsevier Inc., 2017.

CHAPTER 4

METHODOLOGY AND EXPERIMENTATION

4.1 Materials

Precursors used in the synthesis of NaNiF_3 and its composite are Sodium Fluoride (Sigma Aldrich, $\geq 99\%$, CAS Number 7681-49-4), Nickel Chloride Hexahydrate (Sigma Aldrich, $\geq 98\%$, CAS Number 7791-20-0), MWCNT are purchased commercially. Ethanol (Analytical grade) and DI water are used as a solvent in Synthesis.

4.2 Synthesis of NaNiF_3

For Synthesis of NaNiF_3 , stoichiometric amounts of NaF (0.906 g) and $\text{NiCl}_2 \cdot 6\text{H}_2\text{O}$ (1.79 g) are used in a chemical reaction, firstly both the precursors are made soluble in 25 ml DI water separately at 60°C at 600 rpm on the hot plate, after both the precursors become completely soluble in DI water, NaF solution is poured into the Nickel Chloride solution, the transparent green solution will start becoming turbid, Stirred it for 6 h at 60°C at 600 rpm on the hot plate to partially evaporate the solvent (DI water) [1], the left out dense light green liquid is transferred to autoclave and placed in the oven for 24 h at 140°C as shown in Fig. 4.1. After cooling down, light green settled material is washed 3 times with DI water to remove by-products (NaCl) and unreacted reactant. After washing, the material is air dried in oven 24 hours at 80°C .



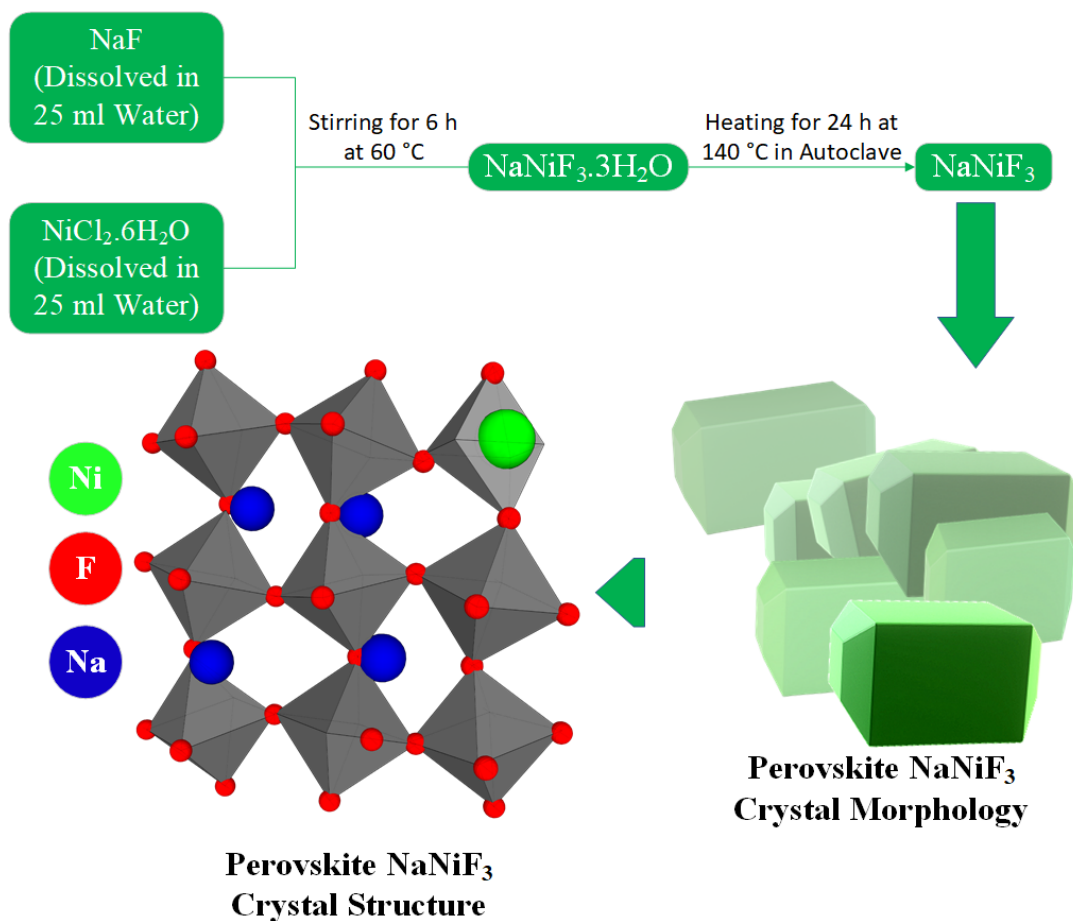


Figure 4.1 Schematic for synthesis of NaNiF₃.

4.3 Synthesis of NaNiF₃ // MWCNT

To make a composite of NaNiF₃ with MWCNT, NaNiF₃ and 20 wt.% of MWCNT are dissolved in about 30 ml of Ethanol and sonicated for 1 hour to completely disperse both the components with each other in the solvent. After Sonication, the solution is placed in an autoclave and placed in the oven for 18 hours at 120°C. After cooling down the settled material is collected and dried for 12 hours at 60°C in a vacuum oven.

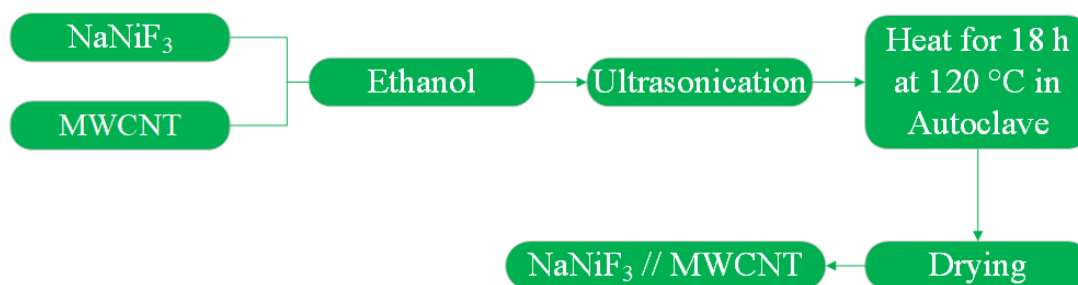


Figure 4.2 Schematic for synthesis of NaNiF_3 composite with MWCNT.

4.4 Material Characterization

The phase analysis of synthesized crystal structure is done by X-Ray Diffraction (D8 Advance by Bruker having $\text{Cu-}\alpha$ as radiation material, Morphology is revealed by Scanning Electron Microscopy (VEGA 3LMU, TESCAN), Chemical composition is analyzed by EDS. For thermogravimetric Analysis, DTG-60/60H instrument is used to analyze the thermal degradation profile and also to confirm the wt.% of MWCNT in the composite sample. The surface area and porosity of synthesized material are analyzed by Brunauer-Emmett-Teller analysis using NovaWin 20e instrument.

4.5 Electrochemical Characterization

For electrochemical characterization, we used 3 electrodes based electrochemical workstation (CH Instruments, USA) CHI 760E, which include platinum wire as a counter electrode, Ag/AgCl as reference electrode, and glassy carbon electrode as working electrode. 1 M Na_2SO_4 is used as an electrolyte for electrochemical measurements. Within the voltage range of 0 V to 1 V, cyclic voltammetry analysis is performed at different sweep speeds of 5 mV s^{-1} , 10 mV s^{-1} , 20 mV s^{-1} , and 50 mV s^{-1} . Chronopotentiometry technique was used to evaluate the galvanostatic charge/discharge, for each sample, five cycles at each current density of 0.1 A g^{-1} , 0.5 A g^{-1} , and 1 A g^{-1} were performed, measurements were made in the potential range of 0 V to 1 V. Electrochemical impedance spectroscopy is carried out between the frequencies of 1 Hz and 1 Mhz.

Summary:

In this chapter, all the experimental process involved in the synthesis of material are explained. The synthesis process of NaNiF_3 and NaNiF_3 //MWCNT and their material characterization techniques and all electrochemical characterization techniques used for testing of electrode material for aqueous sodium ion battery are explained in this chapter.

References:

- [1] E. C. Gonzalo, M. Hoelzel, M. T. Azcondo, U. Amador, F. Garc, and A. Kuhn, "Synthesis and Characterization of $\text{NaNiF}_3 \cdot 3\text{H}_2\text{O}$: An Unusual Ordered Variant of the ReO_3 Type," 2015.

CHAPTER 5

RESULTS & DISCUSSION

5.1 Material Characterization

5.1.1 X-Ray Diffraction

The phase analysis and crystallinity parameters obtained from X-Ray diffraction data of NaNiF_3 confirms the orthorhombic perovskite structure with space group of pnma (62) matching with JCPDS card no. 70-2401 [1] shown in Figure 5.1., the observed peaks at 23.0, 32.30, 32.81, 33.304, 37.14, 38.848, 47.11, 52.37, 54.08, 57.95, 59.24 and 68.84 have (101), (200), (121), (002), (102), (112), (202), (301), (222), (321), (123) and (242) planes respectively, which reveal the formation of perovskite structure of synthesized NaNiF_3 . XRD of MWCNT shows their characteristic peaks at 26.005 and 44.204 have (002) and (100) planes respectively. The XRD of $\text{NaNiF}_3 // \text{MWCNT}$ shows slight diffraction in peaks as compared with prepared NaNiF_3 and also the characteristic peaks of MWCNT can be observed in Pattern. Crystal size calculates based on XRD data is found to be 23 nm and 2 nm 1 for NaNiF_3 and $\text{NaNiF}_3 // \text{MWCNT}$ respectively. The decrease in crystal size of $\text{NaNiF}_3 // \text{MWCNT}$ can be due to the synthesis process of the addition of MWCNT.

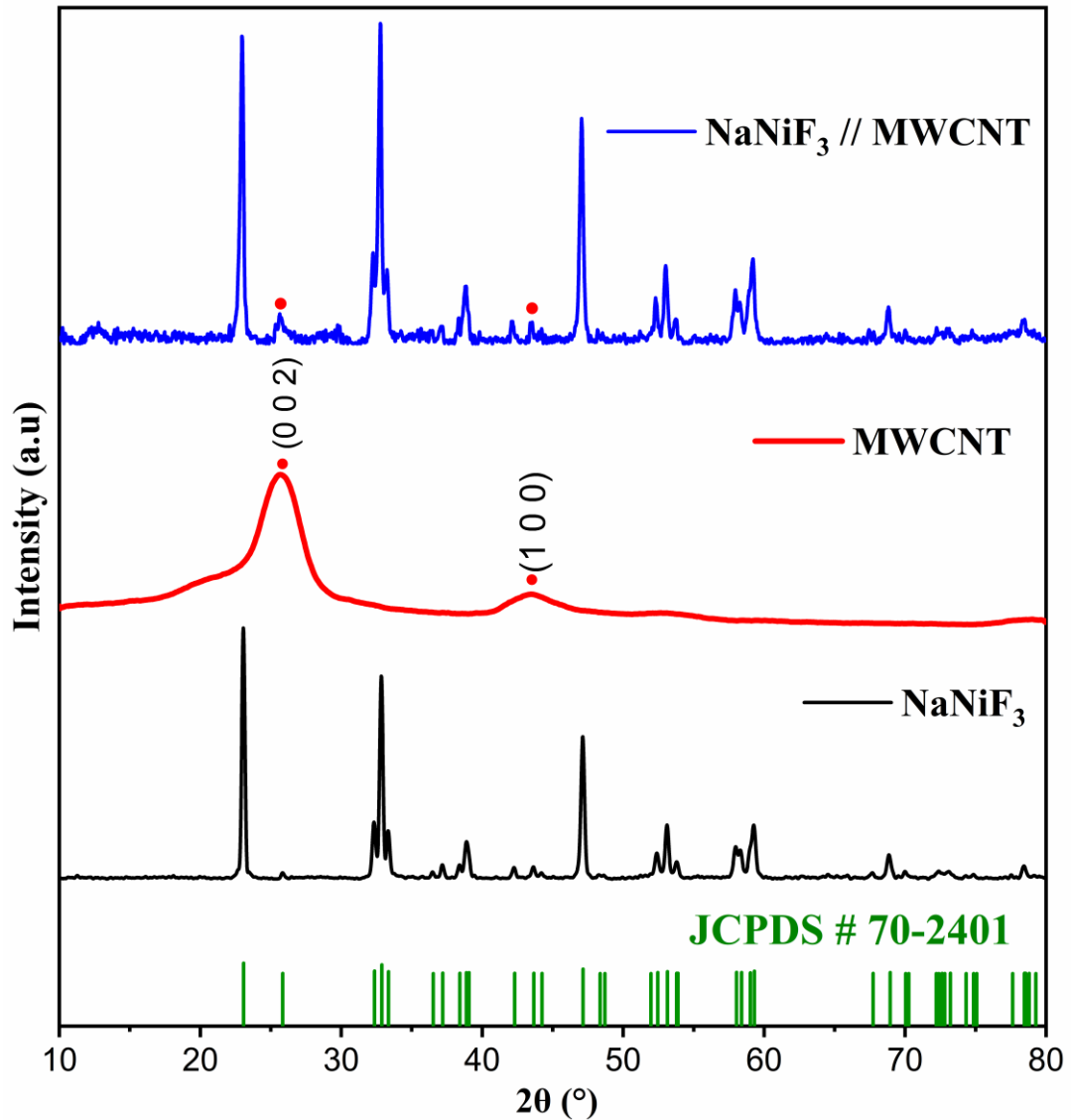


Figure 5.1 XRD patterns of synthesized NaNiF₃, MWCNT, and NaNiF₃ // MWCNT.

5.1.2 Scanning Electron Microscopy

Scanning electron microscopy reveals the morphology of the synthesized Perovskite NaNiF₃, SEM images of NaNiF₃ show the agglomeration of orthorhombic cubical structure which has edged corners at both ends as shown in fig. 5.2 (a, b). While the SEM images of NaNiF₃ // MWCNT show that the shape crystal of NaNiF₃ changes to the cube-shaped crystal after the addition of MWCNT and is surrounded and present in the mesh of MWCNTs as shown in Fig. 5.2 (d). Fig. 5.2 (c) shows the SEM image of MWCNTs used as composite material.

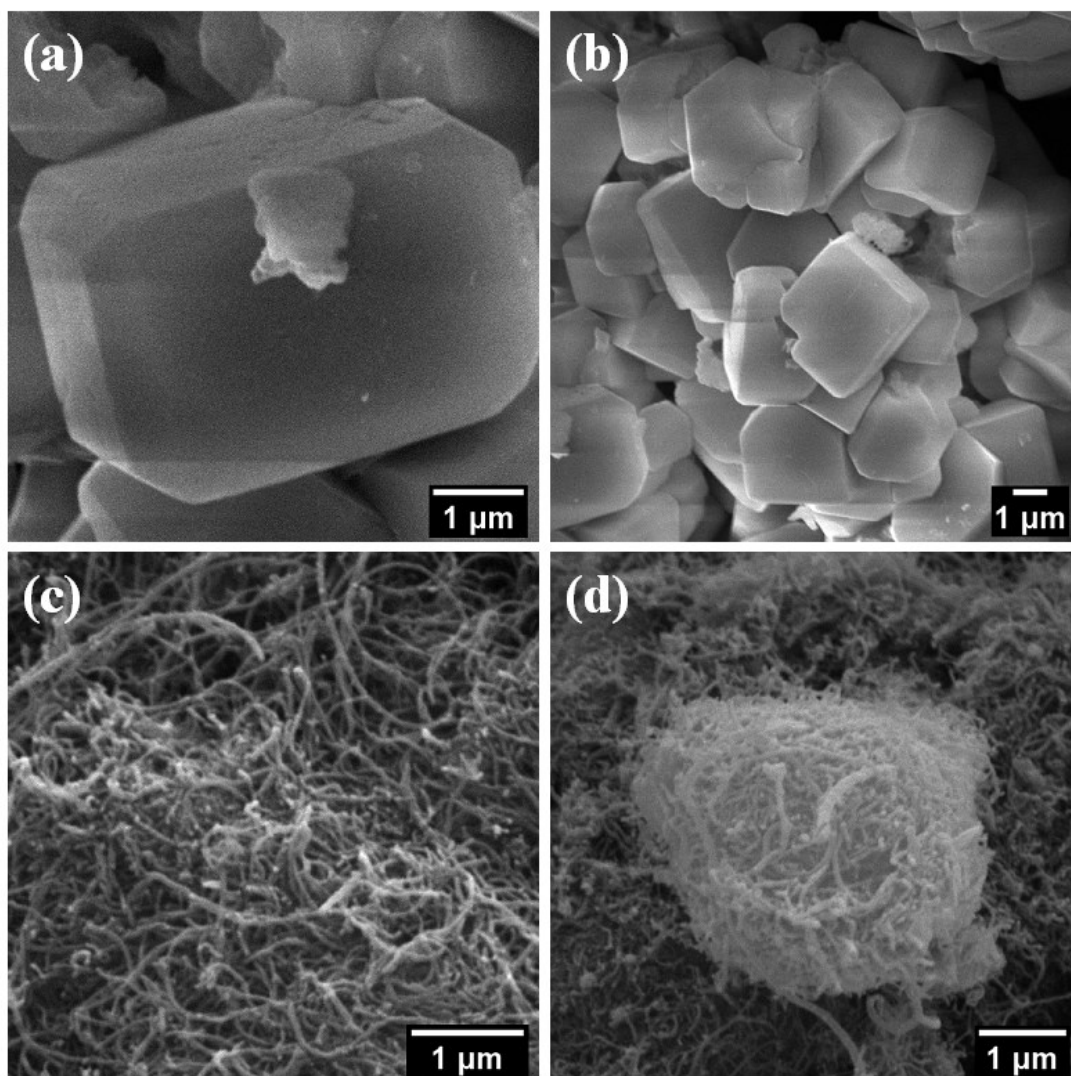


Figure 5.2 SEM images of (a) NaNiF_3 , (b) NaNiF_3 , (c) MWCNT and (d) NaNiF_3 // MWCNT.

5.1.3 Energy Dispersive X-Ray Spectroscopy

EDS spectra of NaNiF_3 and NaNiF_3 // MWCNT revealing the chemical composition are shown in fig. 5.3 (a, b) and table 5.1, which show the atomic percentage of the elements present in the synthesized material, also confirming the relative composition of that of NaNiF_3 and NaNiF_3 // MWCNT (20 wt.%).

Table 5.1 Elemental composition of NaNiF_3 and $\text{NaNiF}_3 // \text{MWCNT}$.

	NaNiF_3	$\text{NaNiF}_3 // \text{MWCNT}$
Element	Weight%	Weight%
C		26.41
F	50.54	45.01
Na	13.24	10.36
Ni	36.22	18.22
Totals	100	100

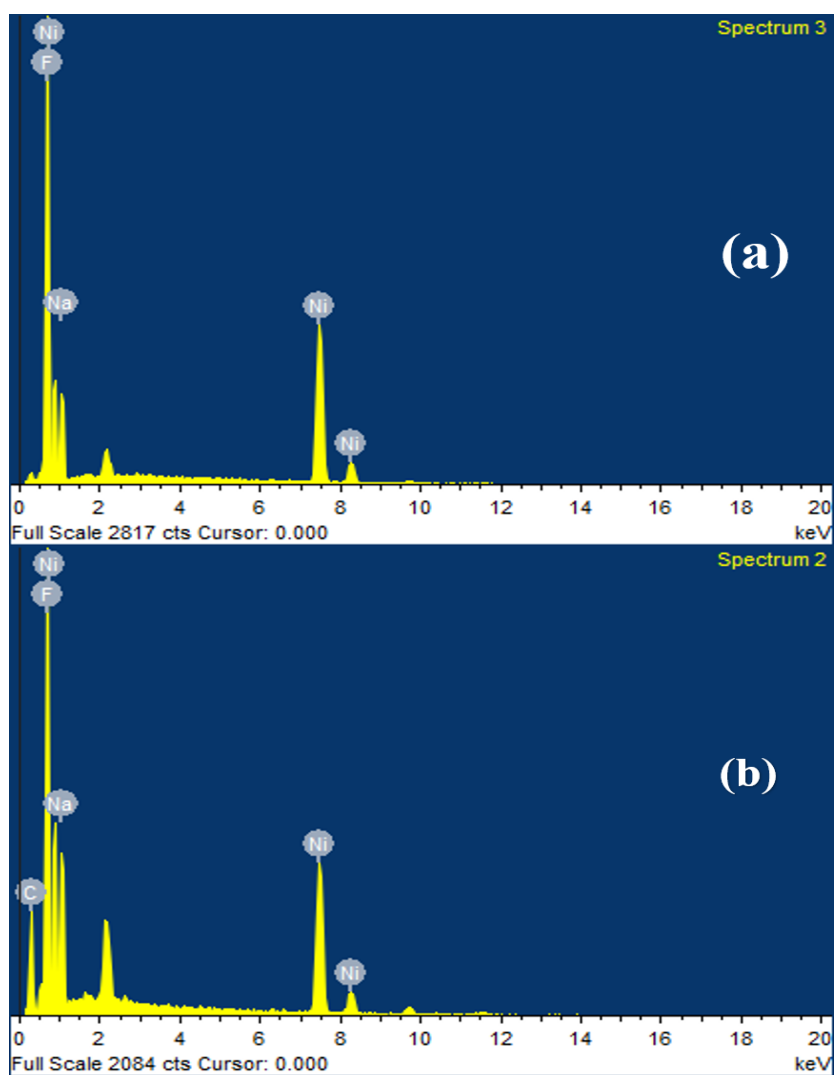


Figure 5.3 EDS spectra of (a) NaNiF_3 , and (b) $\text{NaNiF}_3 // \text{MWCNT}$.

5.1.4 Thermogravimetric Analysis

Thermogravimetric analysis of the synthesized sample was performed from 0-800°C in an inert atmosphere (N₂ atmosphere) at a ramp rate of 10°C min⁻¹, as shown in fig. 4, NaNiF₃ reveals that approximately 11 % weight loss, the TGA pattern shows very little moisture content removal of approximately 2.5 percent from 100°C to 200°C, indicating that no hydration molecules are present in the synthesized material. [2], the remaining 8.5 percent weight loss between 300°C and 700°C can be ascribed to the breakdown of any organic contaminants contained in the produced substance [1]. The TGA pattern of NaNiF₃ / MWCNT composite reveals a total weight loss of approximately 33%, with % weight loss from temperatures 450°C-600°C indicating the degradation of added weight percent MWCNT in NaNiF₃ as a composite material.

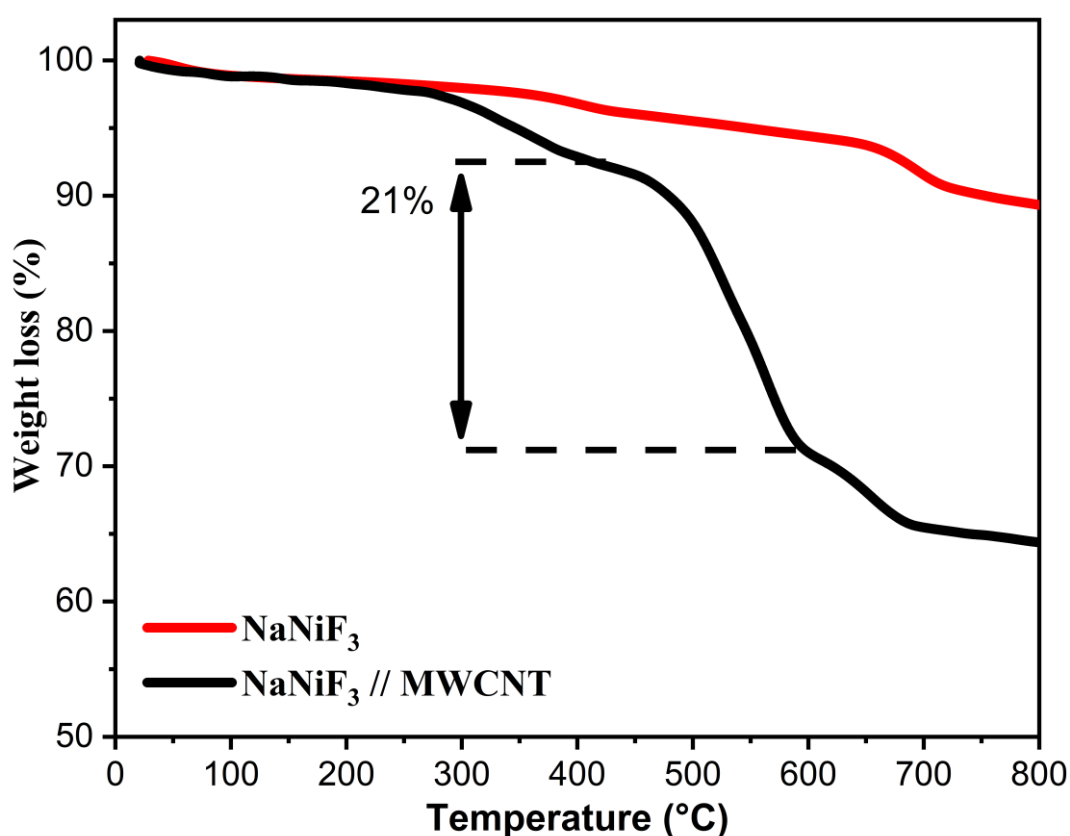


Figure 5.4 Thermogravimetric analysis curves of NaNiF₃ and NaNiF₃ // MWCNT.

5.1.5 BET

The N₂ adsorption-desorption measurements were used to investigate the pore size distribution and specific surface area of as prepared NaNiF₃ and NaNiF₃ // MWCNT, Fig. 5.5 (a), (b) shows the isotherm of both synthesized samples was found

to be of type IV with an H₃ hysteresis loop which confirms the existence of micro and mesoporous in the relative pressure ranges of 0.45-1.0 and 0.7-1.0 respectively, while the inset plot shows the BJH pore size distribution, the surface area of NaNiF₃ and NaNiF₃//MWCNT was found to be 16.6 m² g⁻¹ and 946.9 m² g⁻¹ and the pore volume was 0.0376 cm³ g⁻¹ and 3.08 cm³ g⁻¹ respectively. The enhanced surface area of NaNiF₃//MWCNT can be attributed to the presence of MWCNT in the sample, also due to which the pore volume increases.

Table 5.2 BET Pore volume, surface area and average pore radius of NaNiF₃ and NaNiF₃//MWCNT.

Electrode Material	Surface Area (m² g⁻¹)	Pore volume (cm³ g⁻¹)	Average Pore Radius (nm)
NaNiF₃	16.6	0.037	1.8
NaNiF₃//MWCNT	916.9	3.08	1.7

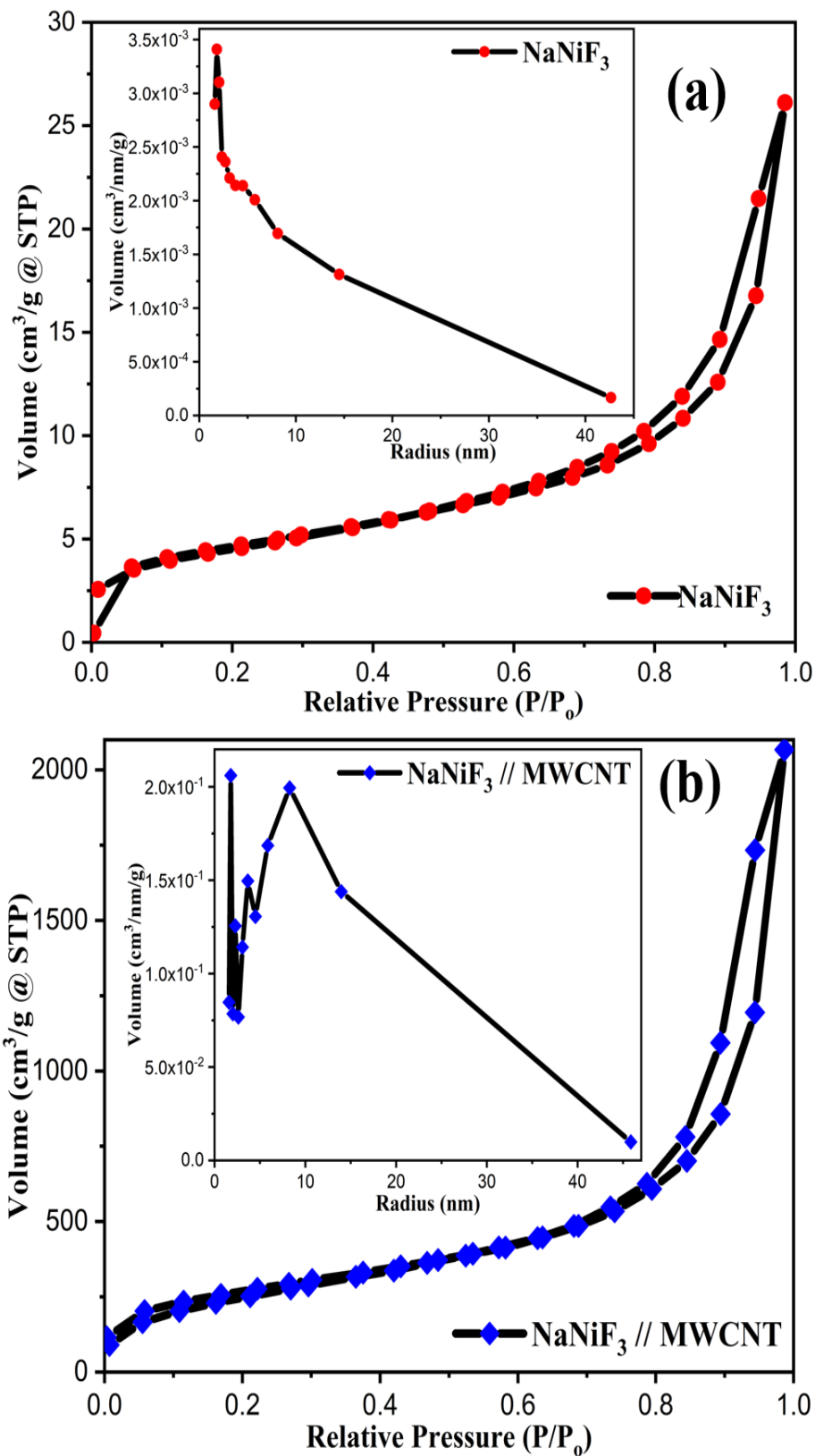


Figure 5.5 N₂ Adsorption-desorption isotherms (inset graph of BJH pore size distribution) of (a) NaNiF₃ and (b) NaNiF₃ // MWCNT.

5.2 Electrochemical Characterization

5.2.1 Cyclic Voltammetry

To study the electrochemical behavior, cyclic voltammetry was performed on prepared NaNiF_3 and $\text{NaNiF}_3/\text{MWCNT}$ composites in 1 M Na_2SO_4 electrolyte. Cyclic Voltammograms were recorded at sweep rates of 5 mV s^{-1} , 10 mV s^{-1} , 20 mV s^{-1} , and 50 mV s^{-1} were used. In all CVs, the anodic peak observed between 0.6 V-0.9 V corresponds to the process of Na^+ -Ion's intercalation, while in the Cathodic peaks from 0.8 V – 0.5 V corresponds to the process of Na^+ -ions deintercalation. For both NaNiF_3 and $\text{NaNiF}_3 // \text{MWCNT}$ cyclic voltammograms are shown in fig. 5.6 (a), (b), the electrochemical kinetics of synthetic materials are studied using CV curves at various sweep rates. , for NaNiF_3 , the area of CV curve increased with increasing sweep rate, with the increase in oxidation peak shifting towards low potential and increase in reduction peak shifting towards high potential, while for $\text{NaNiF}_3 // \text{MWCNT}$ area of CV increases with the increase in sweep rate, with the increase in oxidation peak shifting toward the low potential, while in the reduction shows the increase in the number of reduction peaks to two as compared with NaNiF_3 which indicates the more deintercalation of Na^+ -Ions from the material which can be attributed to a slight change in the morphology of $\text{NaNiF}_3 // \text{MWCNT}$. Fig. 5.6 (c) shows the CV comparison between NaNiF_3 and its composite with MWCNTs.

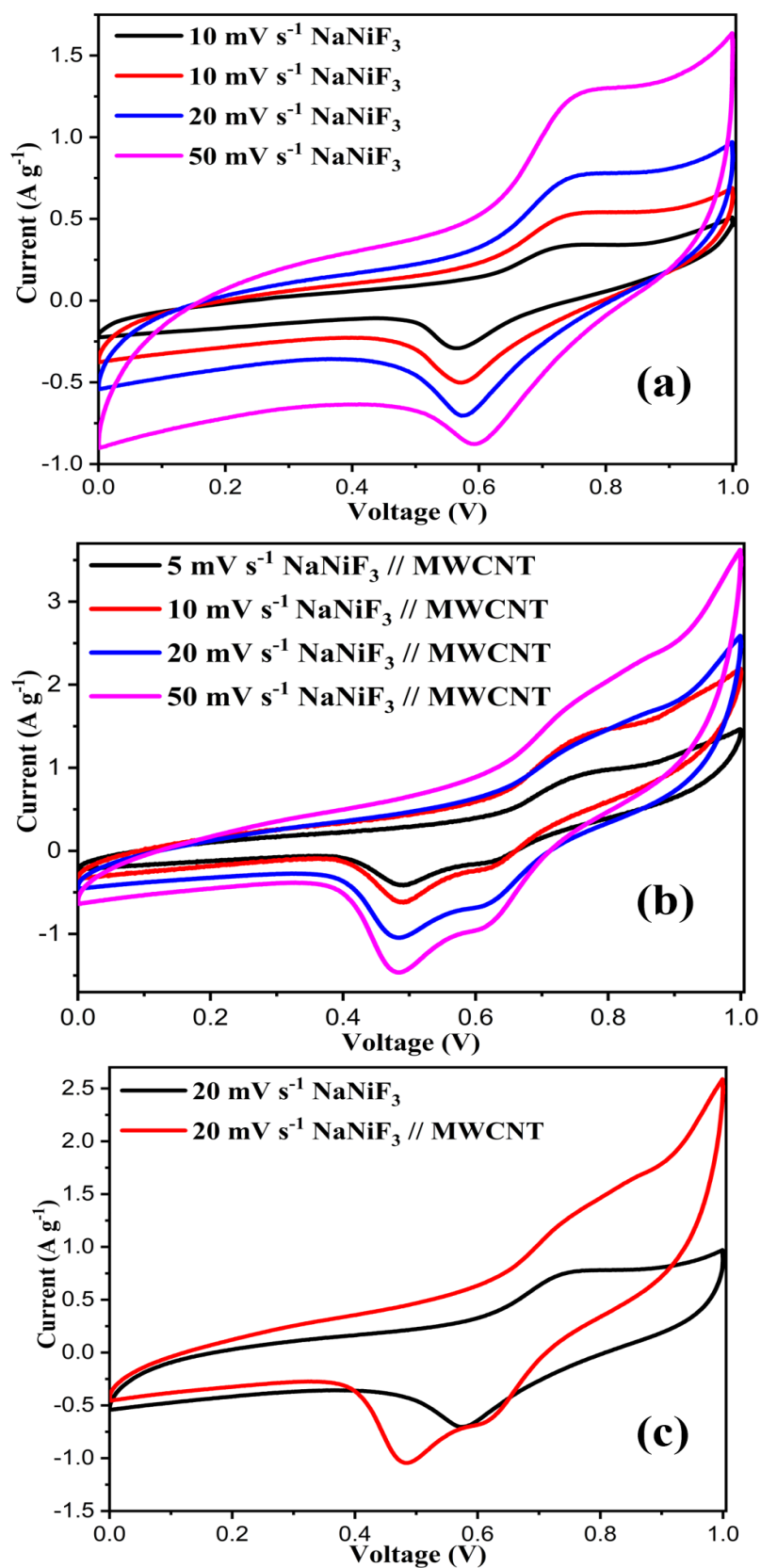


Figure 5.6 Cyclic Voltammetry curves of (a) NaNiF₃, (b) NaNiF₃ // MWCNT and (c) Comparison of CV of NaNiF₃ and NaNiF₃ // MWCNT.

5.2.2 Chronopotentiometry

The charge-discharge behavior of synthetic materials was studied using the chronopotentiometry approach. Fig. 5.7 (a), (b) represents the charge discharge curves of NaNiF_3 and $\text{NaNiF}_3 // \text{MWCNT}$. The Specific capacity is calculated from the following formula [4].

$$\text{Specific Capacity} \left(\frac{\text{mAh}}{\text{g}} \right) = \frac{1}{3.6} * \frac{\text{Discharge time (s)} * \text{Current(A)}}{\text{Mass Loading (g)}} \quad \dots (2)$$

At each current density of 1 A g^{-1} , 0.5 A g^{-1} , and 0.1 A g^{-1} for NaNiF_3 , the calculated discharge capacities are 33.3 mAh g^{-1} , 21.66 mAh g^{-1} , 15.62 mAh g^{-1} , while for $\text{NaNiF}_3 // \text{MWCNT}$ these are 57.08 mAh g^{-1} , 31.18 mAh g^{-1} and 22.45 mAh g^{-1} respectively. Fig. 5.7 (c) shows the comparison of charge-discharge behavior of both NaNiF_3 and $\text{NaNiF}_3 // \text{NaNiF}_3 // \text{MWCNT}$. The result shows the increase in discharge capacity of $\text{NaNiF}_3 // \text{MWCNT}$ as compared with that of NaNiF_3 which can be attributed to the increase in electronic conductivity and ionic conductivity in $\text{NaNiF}_3 // \text{MWCNT}$ as compared with NaNiF_3 . The energy density calculated for NaNiF_3 was 16 Wh kg^{-1} , which increases to 28.5 Wh kg^{-1} for $\text{NaNiF}_3 // \text{MWCNT}$.

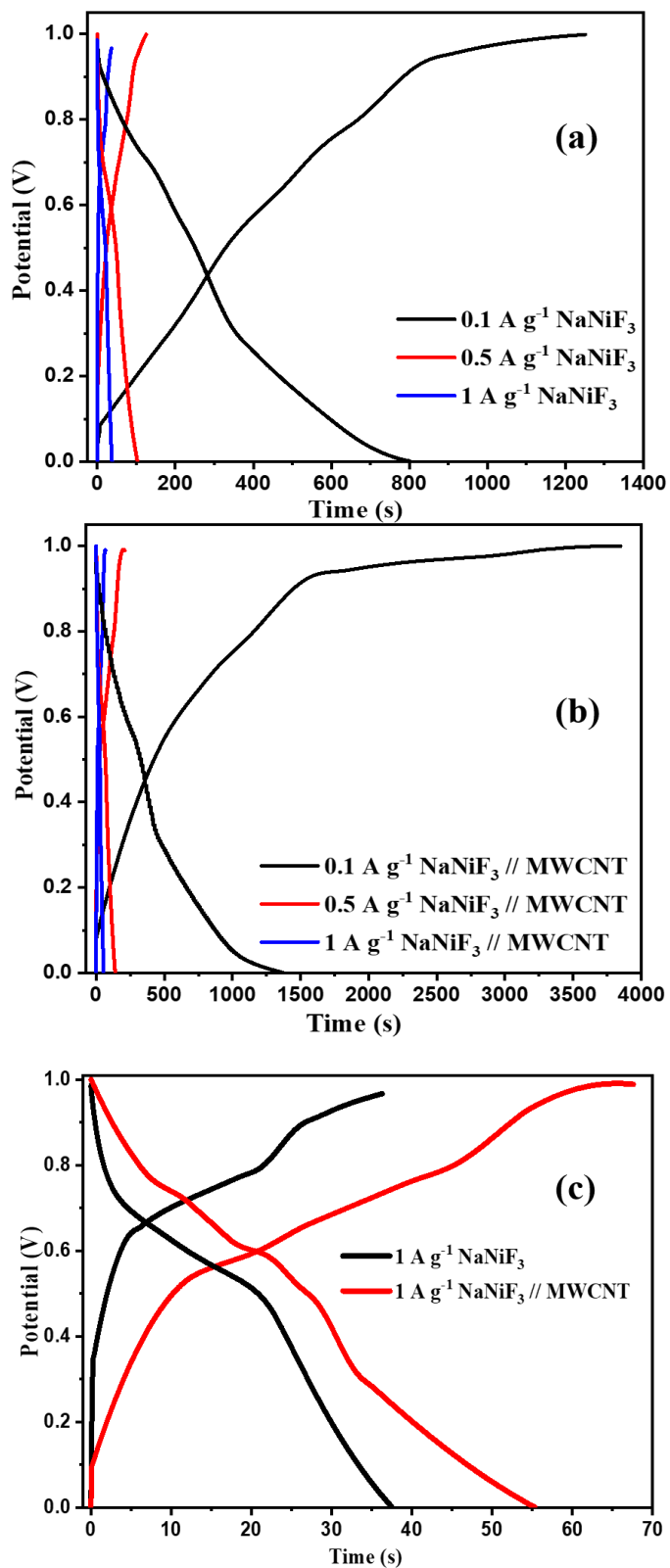


Figure 5.7 . Represents the galvanic charge-discharge curves of (a) NaNiF_3 (b) $\text{NaNiF}_3 // \text{MWCNT}$, (c) GCD curve comparison between NaNiF_3 and $\text{NaNiF}_3 // \text{MWCNT}$.

5.2.3 Electrochemical Impedance Spectroscopy

To reveal the reaction kinetics of NaNiF_3 and $\text{NaNiF}_3 // \text{MWCNT}$ Electrochemical Impedance Spectroscopy was done in the range of 1 Hz to 1 MHz. Nyquist plot is plotted and data is fitted with an equivalent circuit shown in fig. 5.8 (a). The resistance R_s corresponds to electrolyte resistance, R_1 and R_2 resistors parallel with the capacitor, and constant phase element (Q) corresponds to the contact impedance and charge transfer impedance. The ion diffusion in the host material corresponds to Warburg Element (W). Values of different resistances obtained from the equivalent circuit fitter data are mentioned in Table 5.2, Electrolyte resistances (R_s) are the same for both of the materials, while the contact impedance for NaNiF_3 is higher than $\text{NaNiF}_3 // \text{MWCNT}$ due to its more surface area, while increase in charge transfer resistance indicates the high ion diffusion and more volume changes than NaNiF_3 . Fig. 5.8 (b) represents the bode plot corresponding to the Na^+ diffusion within the electrode material, the low-frequency contribution of $\text{NaNiF}_3 // \text{MWCNT}$ shifted higher as compared with that of NaNiF_3 which indicated the more diffusion of Na^+ ion through the electrode material.

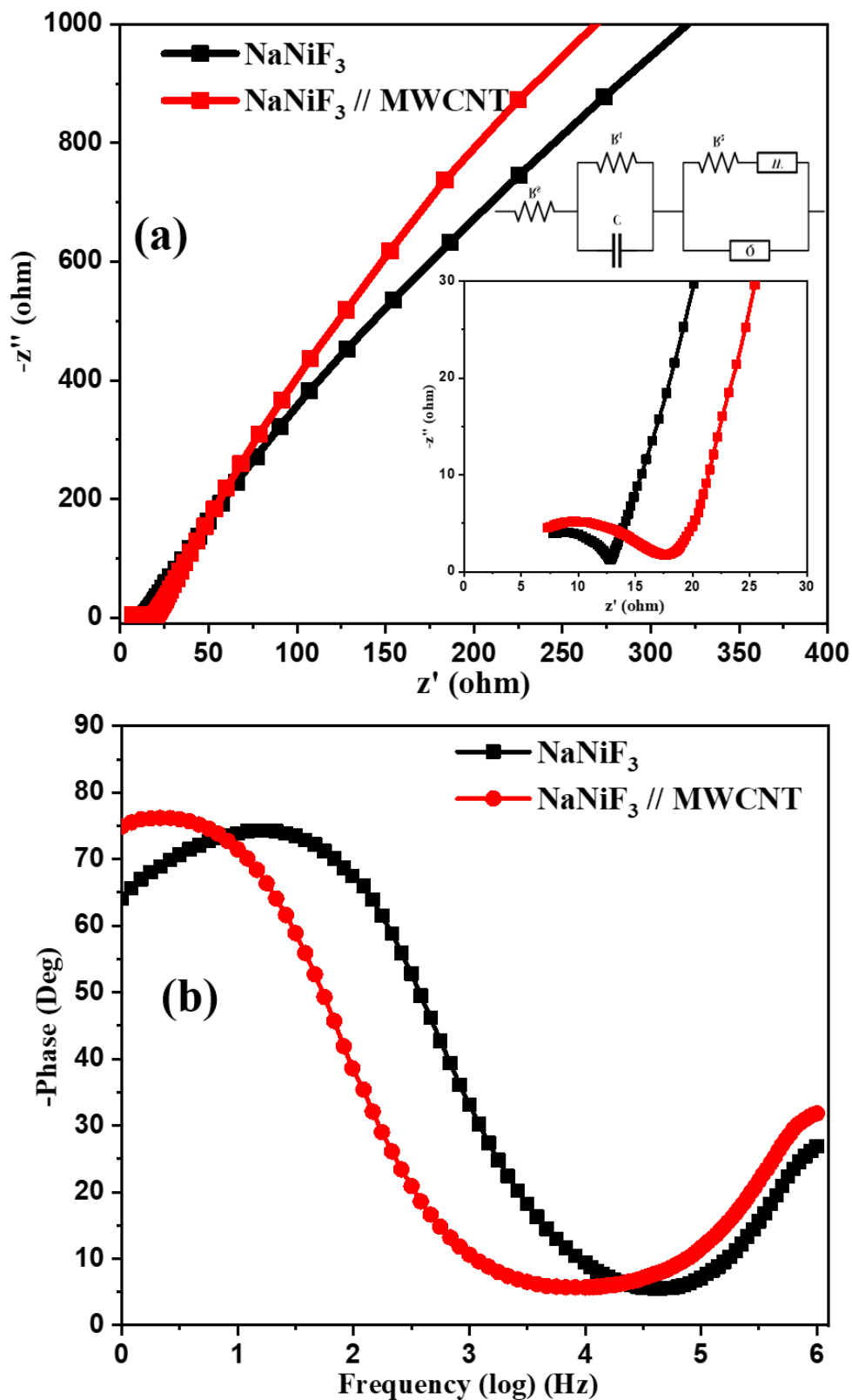


Figure 5.8 Represents the electrochemical impedance spectroscopy (a) Nyquist plot of NaNiF_3 and $\text{NaNiF}_3 // \text{MWCNT}$ with inset equivalent fitted circuit and (b) Bode plot of NaNiF_3 and $\text{NaNiF}_3 // \text{MWCNT}$.

5.2.4 Cyclic Stability

For each scan rate of 1 A g^{-1} , 0.5 A g^{-1} , and 0.1 A g^{-1} , the initial five cycles of charge discharge behaviour were recorded. for both NaNiF_3 and $\text{NaNiF}_3 // \text{MWCNT}$ are recorded as shown in Fig. 5.9 (a). Cyclic stability of both the materials are tested for 500 cycles at a high scan rate of 1 A g^{-1} as shown in fig. 5.9 (b), NaNiF_3 shows a slight increase in discharge capacity in the initial 20 cycle and then becomes constant, while $\text{NaNiF}_3 // \text{MWCNT}$ composite shows a very slight increase in initial 10 cycles then start decreasing in discharge capacity and decreases to about 92% till 500th cycle, which can be due to high deintercalation of Na^+ -ions as compared to NaNiF_3 .

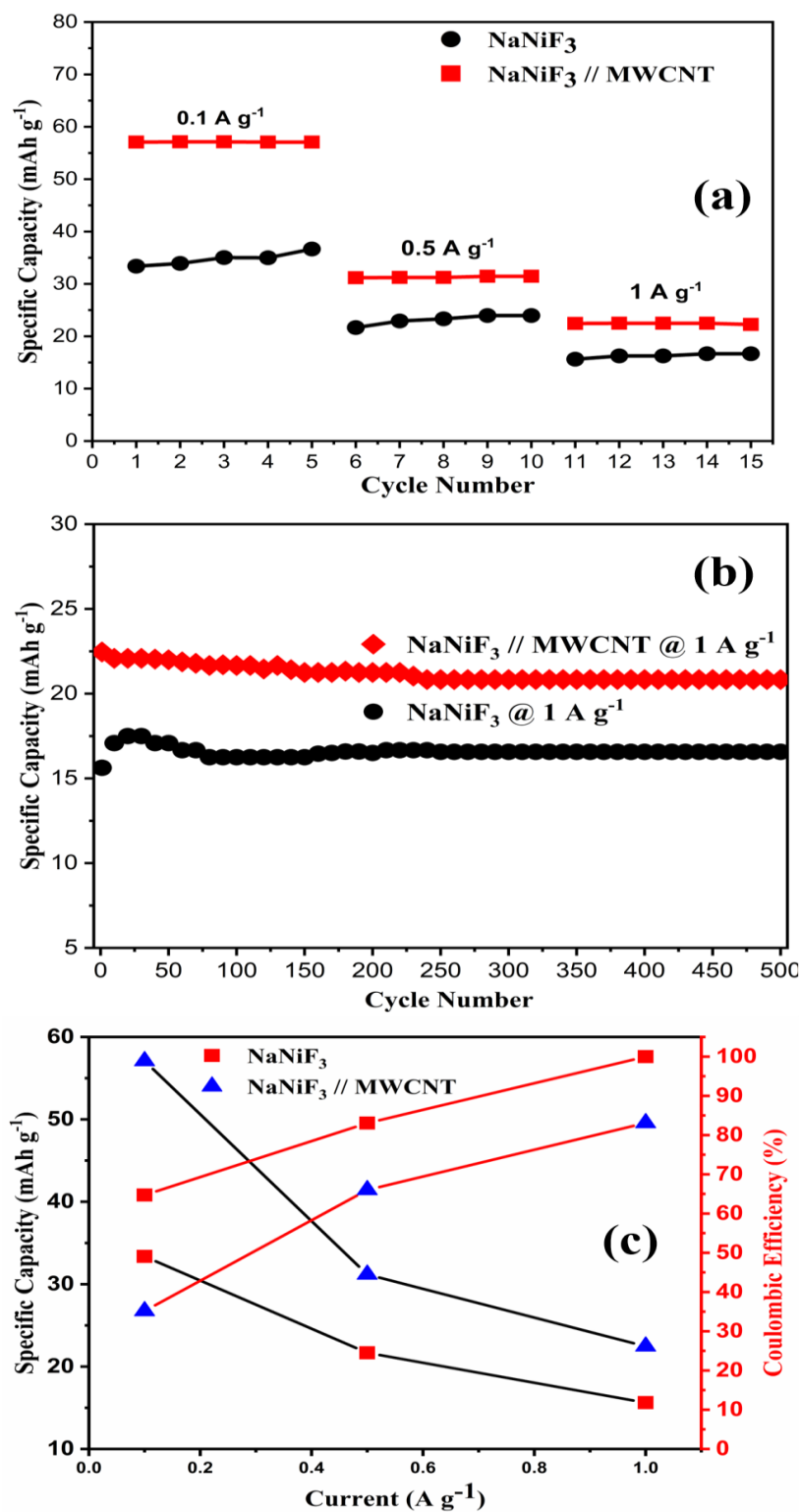


Figure 5.9 (a) Specific capacitance at each scan rate for initial 5 cycles each of NaNiF₃ and NaNiF₃ // MWCNT (b) Cyclic stability at 1 A g⁻¹ of NaNiF₃ and NaNiF₃ // MWCNT (c) Comparison of specific capacity and coulombic efficiency at each scan rate of NaNiF₃ and NaNiF₃ // MWCNT.

5.3 Discussion

Besides having a high operating voltage, high energy density and perovskite structure, one of the major reasons for not exploring the Sodium Transition metal fluoride was their complex synthesis routes and their low conductance in electrochemical energy storage systems, here in this study, we have successfully synthesized Sodium Transition Metal Fluoride (NaNiF_3) by low cost and safe precipitation and hydrothermal route and its composite with MWCNT to increase its electronic conductivity and tested it for the application of the aqueous sodium-ion battery. The most commonly used cathode materials for Aqueous Sodium-ion batteries are Transition Metal Oxides, Prussian Blue Analogues, Polyanionic Compounds, and Organic Polymers. Herein in we have introduced Sodium Transition Metal Fluorides (NaNiF_3) as cathode material for Aqueous Sodium-Ion Battery, $\text{NaNiF}_3 // \text{MWCNT}$ shows the good cathodic performance having a specific capacity of 57.06 mAh g^{-1} at 0.1 A g^{-1} , having good cyclic stability of 92% for 500 cycles with a 28.5 Wh kg^{-1} energy density. Table 4 shows recent advancements in cathode materials for Aqueous sodium-ion batteries, a relative comparison of recent advancements of cathode material for aqueous sodium-ion battery with this study shows that Sodium Transition Metal Fluorides $\text{NaNiF}_3 // \text{MWCNT}$ is the promising cathode material and they have the great potential for the application of Aqueous Sodium-Ion Battery.

Table 5.3 Comparison of this study with recent literature.

Sr. No.	Material	Electrolyte	Discharge Capacity / Rate	Retention Capacity (%)	Cycles	Ref.
1	NaNiF ₃ // MWCNT	1 M Na ₂ SO ₄	57.06 mAh g ⁻¹ @ 1 A	92	500	This Work
2	NiHCF	1 M NaNO ₃	76 mAh g ⁻¹ @ 1 C	93	1000	[5]
3	Na _{0.44} MnO ₂	6 M NaNO ₃	123.5 mAh g ⁻¹ @1 A			[4]
4	Na ₂ VTi- (PO ₄) ₃ @ C	5 M NaClO ₄	52.4 mAh g ⁻¹ @ 1C			[6]
5	Na _{0.44} MnO ₂ - CNT	1 M Na ₂ SO ₄	70 mAh g ⁻¹ @ 50 mA g ⁻¹	53.1	300	[7]
6	Na _{0.57} CoO ₂	0.5 M Na ₂ SO ₄	57 mAh g ⁻¹ @0.7C	79	1000	[8]
7	Na ₃ MnCO ₃ PO ₄	5 M NaNO ₃	77.05 mAh g ⁻¹ @0.2 C	89	50	[9]

Summary:

In this Chapter, all the results obtained by the research are discussed, characterization of material including XRD, SEM, EDS, TGA and BET are discussed and supported with facts and justified to understand the phase, structure, morphology, Composition, surface area, pore size and thermal stability of synthesized material. Cyclic voltammetry, chronopotentiometry, and electrochemical impedance spectroscopy are used to characterize the material electrochemically which unveils the potential of synthesized material as a possible cathode material for an aqueous sodium-ion battery and their link with characterization properties is justified and compared with recent literature work.

References:

- [1] N. Hussain, F. Wu, W. Younas, and L. Xu, “Hollow sphere formation by the self-aggregation of perovskite fluoride NaNiF_3 nanocrystals and the application of these spheres as an electrode in an ultrahigh performance asymmetric supercapacitor,” *New J. Chem.*, vol. 43, no. 30, pp. 11959–11967, 2019.
- [2] E. C. Gonzalo, M. Hoelzel, M. T. Azcondo, U. Amador, F. Garc, and A. Kuhn, “Synthesis and Characterization of $\text{NaNiF}_3 \cdot 3\text{H}_2\text{O}$: An Unusual Ordered Variant of the ReO_3 Type,” 2015.
- [3] S. Li, Y. Yang, M. Xie, and Q. Zhang, “Synthesis and electrochemical performances of high-voltage $\text{LiNi}_{0.5}\text{Mn}_{1.5}\text{O}_4$ cathode materials prepared by hydroxide co-precipitation method,” *Rare Met.*, vol. 36, no. 4, pp. 277–283, 2017.
- [4] L. Rakočević, S. Štrbac, J. Potočnik, M. Popović, D. Jugović, and I. S. Simatović, “The Na_xMnO_2 materials prepared by a glycine-nitrate method as advanced cathode materials for aqueous sodium-ion rechargeable batteries,” *Ceram. Int.*, vol. 47, no. 4, pp. 4595–4603, 2021.
- [5] S. Park, J. Kim, S. H. Yi, and S. E. Chun, “Coprecipitation Temperature Effects of Morphology-Controlled Nickel Hexacyanoferrate on the Electrochemical Performance in Aqueous Sodium-Ion Batteries,” *ChemSusChem*, vol. 14, no. 4, pp. 1082–1093, 2021.
- [6] L. Shen *et al.*, “NASICON-Structured $\text{Na}_2\text{VTi}(\text{PO}_4)_3@C$ for Symmetric Aqueous Rechargeable Na-Ion Batteries with Long Lifespan,” *ACS Sustain. Chem. Eng.*, vol. 9, no. 9, pp. 3490–3497, 2021.
- [7] F. Gu, T. Sun, X. Yao, M. Shui, and J. Shu, “Studies on the improved electrochemical performance and the sodium ion migration mechanism of $\text{Na}_{0.44}\text{MnO}_2$ -CNT electrodes for aqueous sodium batteries,” *J. Phys. Chem. Solids*, vol. 149, no. July 2020, p. 109771, 2021.
- [8] A. C. Nwanya, M. M. Ndipingwi, F. I. Ezema, E. I. Iwuoha, and M. Maaza, “Bio-synthesized $\text{P}_2\text{-Na}_{0.57}\text{CoO}_2$ nanoparticles as cathode for aqueous sodium ion battery,” *J. Electroanal. Chem.*, vol. 878, p. 114600, 2020.

- [9] K. Shiprath, H. Manjunatha, K. C. Babu Naidu, A. Khan, A. M. Asiri, and R. Boddula, "Na₃MnPO₄CO₃ as cathode for aqueous sodium ion batteries: Synthesis and electrochemical characterization," *Mater. Chem. Phys.*, vol. 248, no. March, p. 122952, 2020.

CHAPTER 6

CONCLUSION AND RECOMENDATIONS

6.1 Conclusion

Here in this work, we have successfully synthesis the NaNiF_3 by the combination of precipitation and hydrothermal method followed by the synthesis of its composite with MWCNT, detailed structural, morphological, chemical, and electrochemical analysis was performed. The perovskite structure phase of NaNiF_3 was confirmed by XRD. Crystal morphology revealed by SEM of NaNiF_3 shows the Orthorhombic cube structure with edged corners at both ends, while the morphology of $\text{NaNiF}_3 // \text{MWCNT}$ was cube-shaped crystals surrounded and present in the mesh of MWCNT. Electrochemical properties of NaNiF_3 and its composite with MWCNTs for the application of aqueous sodium-ion battery was tested by cyclic voltammetry, chronopotentiometry, and electrochemical impedance spectroscopy, which show the specific discharge capacity of about 33 mAh g^{-1} and 57.06 mAh g^{-1} of NaNiF_3 and $\text{NaNiF}_3 // \text{MWCNT}$ respectively with a retention capacity of 92% for 500 cycles and have the energy density of 16 Wh kg^{-1} & 28.5 Wh kg^{-1} of NaNiF_3 and $\text{NaNiF}_3 // \text{MWCNT}$ respectively, which shows that $\text{NaNiF}_3 // \text{MWCNT}$ as a potential candidate among cathode materials of aqueous sodium-ion battery.

6.2 Recommendations

The electrochemical performance and efficiency of aqueous sodium ion battery for energy storage applications can be increased by exploring new combinations of materials to be employed as electrodes, in addition to the informed selection of electrolytes to increase the electrochemical potential window. The following recommendations are presented to address the shortcomings in the research regarding the electrode materials for supercapacitors:

- Focus of the future research should be towards the various other transition metals and their composites to be used as efficient electrode materials for aqueous sodium ion battery.
- Exploring of various other stable electrolyte as aqueous electrolyte which can enhance the electrochemical potential window.
- Anode/cathode material reaction with water or O_2 , H_2/O_2 evolution reactions, dissolution of anode/cathode material in water occurs in aqueous electrolyte in aqueous sodium ion battery which ultimately decreases the capacity of battery should be taken into consideration for future research.

Acknowledgments

All praise to Allah Almighty, who gave me the strength to successfully complete this dissertation. Completion of MS Degree has been a challenging, yet interesting journey filled with life lessons. As my research has been completed, I would like to take this opportunity to express sincere gratitude to my supervisor **Dr. Naseem Iqbal** for providing this opportunity, for his teaching and mentorship and continuous support and guidance throughout the MS program and research. I would also like to thank my guidance and evaluation committee: **Dr. Ghulam Ali, Dr. Mustafa Anwar** and **Dr. Sehar Shakir** for their valuable feedback and insights which added value to this research.

I also appreciate the support of teaching and non-teaching faculty of U.S.-Pakistan Center for Advanced Studies in Energy for all the things that facilitated smooth work of my research.

I would particularly acknowledge the immense support of my dear parents **Sheikh Amjad Ali** and **Tayyaba Amjad** who are like beacons of hope throughout this entire journey. I would also admire the wholehearted help of my friends and colleagues who always cheered for me and offered their support in every way possible.

Muhammad Zain Bin Amjad

Appendix 1-Publications

Synthesis of NaNiF_3 and its Composite with Multi-Walled Carbon Nanotubes as Cathode Materials for Aqueous Sodium-Ion Battery

M. Zain Bin Amjad, Naseem Iqbal, Ghulam Ali, Tayyaba Noor, Ahmed A. Qayyum, Usman Ali Khan, Waqas Nazar

Abstract:

Aqueous sodium-ion battery is a safe and efficient system for large scale energy storage due to low cost, abundant sodium supply, non-flammable aqueous neutral electrolyte and quick charge-discharge performance. The use of fluoride-based material as electrode material has a certain advantage due to high potential window and energy density. Exploring perovskite materials has advantage of corner-sharing matrix structure which helps in easy ion and electron diffusion. Herein, we synthesized the perovskite structured NaNiF_3 and its composite with multi-walled carbon nanotubes (MWCNT) by a simple and cost-effective approach by the combination of precipitation and hydrothermal route. The synthesized material is characterized by X-rays Diffractometry (XRD), Scanning Electron Microscopy (SEM), Energy Dispersive X-Ray (EDX), Thermogravimetric Analysis (TGA), and Brunauer-Emmett-Teller analysis (BET). Electrochemical performance for aqueous sodium-ion batteries is tested by cyclic voltammetry (CV), chronopotentiometry (CP), and Electrochemical Impedance Spectroscopy (EIS) in 1 M Na_2SO_4 Electrolyte. XRD confirms the perovskite structure of NaNiF_3 and $\text{NaNiF}_3 // \text{MWCNT}$, SEM shows the orthorhombic cube and cubical structure of NaNiF_3 and $\text{NaNiF}_3 // \text{MWCNT}$. Electrochemical results demonstrate the excellent performance with a specific capacity of 33 mAh g^{-1} and 57.06 mAh g^{-1} at 0.1 A g^{-1} , energy density of 16 Wh kg^{-1} and 28 Wh kg^{-1} for NaNiF_3 and $\text{NaNiF}_3 // \text{MWCNT}$ respectively, and shows excellent cyclic stability up to 500 cycles, indicating that $\text{NaNiF}_3 // \text{MWCNT}$ as potential candidate as cathode material of aqueous sodium-ion battery.

Keywords: Aqueous Sodium-Ion Battery, Sodium Metal Fluoride, Transition Metal Fluoride, Sodium-ion Battery, Cathode Material.

Journal: Electroanalytical Chemistry (IF=4.4) (Under-Review)